Dissertation

Cone Spline Surfaces and Spatial Arc Splines

ausgeführt zum Zwecke der Erlangung des akademischen
Grades eines Doktors der technischen Wissenschaften

eingereicht an der Technischen Universität Wien
Technisch-Naturwissenschaftliche Fakultät

von

Stefan Leopoldseder
Lange Gasse 44/24, 1080 Wien – Matr.Nr. 8926793

geboren am 7. Juli 1971 in Freistadt, OÖ

Wien, im Oktober 1998

Abstract

The design of developable surfaces is of fundamental importance for many applications in Computer Aided Geometric Design. The aim of this thesis is to derive different algorithms to approximate developable surfaces by *cone spline surfaces*, which are G^1-surfaces composed of segments of right circular cones. This can be seen as a certain spatial counterpart of approximating a space curve by an *arc spline*. A new algorithm for such an arc spline approximation of space curves in Euclidean 3-space is presented in this work.

The first chapter shows how to approximate a developable surface by smoothly joining pairs of cone segments. It turns out that there exists a one parameter family of cone pairs which join two generators of the developable surface and touch the tangent planes at these generators. Errors of this approximation method are analyzed and several examples are given.

The second chapter presents a different approximation technique with cone spline surfaces. From the given developable surface a set of osculating cones is computed. For each two consecutive osculating cones a smoothly joining cone segment is determined. In special cases there still exists a one parameter set of solutions but in the general case one will have just two complex solution cones. This survey includes an application of this method to the reconstruction of developable surfaces from scattered data.

The third chapter gives a short introduction into 3-dimensional Euclidean Laguerre space. In the isotropic model of this geometry the approximation techniques of chapters 1 and 2 will appear as curve approximation with isotropic arc splines. With tools from isotropic Möbius geometry we will prove the fundamental theorem that there always exists a joining cone of two sufficiently close osculating cones of a developable surface which is real and useful for applications. This result confirms the feasibility of the methods of chapter 2.

Finally, in chapter four we will discuss *osculating arc spline approximation* of twisted curves in Euclidean 3-space. In general, there exist two arcs that smoothly join two osculating circles of a spatial curve. Again the existence of a real and useful solution is proven. Furthermore an algorithm is presented how to segment

the given curve in order to minimize approximation errors. The approximation algorithms are discussed for several examples.

Kurzfassung (German)

Das computerunterstützte Modellieren mit abwickelbaren Flächen (Torsen) besitzt wichtige Anwendungen im Design mit nicht dehnbaren Materialien. Diese Arbeit behandelt verschiedene Methoden eine gegebene Torse durch *Drehkegelsplineflächen* anzunähern. Dies sind Flächen, welche aus Segmenten von Drehkegeln tangentialstetig zusammengesetzt sind. Es besteht eine enge Verwandtschaft zwischen der Approximation mit Drehkegelsplineflächen und räumlicher Kurvenapproximation durch Kreissplines, also Kurven, die tangentialstetig aus Kreisbögen zusammengesetzt sind. Auch für dieses Problem wird ein neues Verfahren vorgestellt.

Das erste Kapitel behandelt die Approximation von Torsen durch tangentialstetige *Drehkegelpaare*. Zu je zwei Erzeugenden einer Torse existiert eine einparametrige Schar von solchen Drehkegelpaaren, welche die Erzeugenden interpolieren und dort die Tangentialebenen der Torse berühren. Weiters werden Fehlerabschätzungen durchgeführt und die Methoden anhand von Beispielen veranschaulicht.

Im zweiten Kapitel wird ein anderes Approximationsschema mit Drehkegelsplineflächen vorgestellt. Von einer gegebenen Torse werden Krümmungsdrehkegel zu einzelnen Erzeugenden berechnet und mit weiteren Drehkegeln glatt zu einer Drehkegelsplinefläche verbunden. Im Gegensatz zu ersterer Methode existieren im allgemeinen nur zwei komplexe Drehkegel, welche zwei Drehkegel berühren. Als Anwendung dieses Algorithmus wird die Flächenrekonstruktion einer Torse aus einer Punktwolke präsentiert.

Das dritte Kapitel beinhaltet zunächst eine kurze Einführung in die dreidimensionale euklidische Laguerre-Geometrie. Im isotropen Modell dieser Geometrie werden die orientierten Drehkegelsplineflächen nämlich als isotrope Kreissplines abgebildet. Dies ermöglicht einen tieferen Einblick in die geometrische Struktur der Methoden aus den ersten beiden Kapiteln. Weiters kann mit Hilfe von Möbiustransformationen leicht gezeigt werden, daß zu zwei genügend nahen Krümmungskegeln einer Torse ein reeller, berührender Drehkegel existiert, sodaß die Brauchbarkeit des Verfahrens aus Kapitel 2 gesichert ist.

Im vierten Kapitel wird schließlich eine Korbbogenkonstruktion für ebene Kurven auf Raumkurven des euklidischen Dreiraums erweitert. An einzelnen Punkten der Raumkurve werden die Krümmungskreise berechnet und durch berührende Kreisbögen zu einem Kreisspline verbunden. Wiederum kann die Existenz eines reellen Kreisbogens bewiesen werden, der die Orientierung der Krümmungskreise erhält. Anhand eines Beispiels wird abschließend ein Segmentierungsalgorithmus vorgestellt, um die auftretenden Approximationsfehler zu minimieren.

Contents

List of Figures

Introduction

In the computer-aided geometric design literature, rising attention is given to developable surfaces because they are surfaces that can be unfolded (developed) into a plane without stretching or tearing. Because of this property, they are of considerable importance to the modeling of surfaces of approximately unstretchable materials, such as paper, leather or thin sheets of metal. Applications in sheet-metal and plate-metal based industries include windshield design, binder surfaces for sheet metal forming processes, aircraft skins, ship hulls and others (see, for example, Mancewicz and Frey [24]). One motivation of this present work comes from a project launched by Odense Steel Shipyard Ltd. and the Department of Mathematics at the Technical University of Denmark which deals with the design and engineering of double curved ship surfaces (see Randrup [41]). There, developable surfaces appear in the manufacturing process of the steel plates.

To include developable surfaces into current CAD/CAM systems, they need to be represented as NURBS surfaces (see, e.g. Farin [10] or Piegl and Tiller [34]). There are basically two approaches to rational developable surfaces. First, one can express such a surface as a tensor product surface of degree $(1, n)$ and solve the nonlinear side conditions expressing the developability. Aumann [1, 2], Frey and Bindschadler [11], Lang and Röschel [21] or Maekawa and Chalfant [23] follow this approach and attach especial importance to controlling the singular points of these surfaces.

Second, one can view the surface as envelope of its one parameter set of tangent planes and thus treat it as a curve in dual projective space. Bodduluri and Ravani [3, 4] were the first to give algorithms similar to deCasteljau and Farin-Boehm for developable surfaces. Further geometric contributions are given by Hoschek [16] and Pottmann [35]. Based on the dual approach, some interpolation and approximation algorithms as well as initial solutions to special applications have been presented recently by Hoschek and Pottmann [17], Hoschek and Schneider [18], Pottmann and Farin [37], Pottmann and Wallner [40], Schneider [46] and Vatter [56]. The numerical computation of the isometric mapping of a developable surface into the plane has been treated by several authors (see e.g. Clements and Leon [9], Gurunathan and Dhande [13], Kreyszig [19] or Weiss and Furtner [55]).

A technique to model developable surfaces with smoothly joined segments of general cones was proposed by Sun and Fiume [53]. For the design of the cross sections of the cone patches B-spline curves are used. One still needs numerical integration to flatten out such a general cone segment, though. Redont [42] uses patches of right circular cones (cones of revolution), their development being elementary. Because of the global methods given in [53, 42], the adjustment of a single cone patch affects the position of all the adjacent patches.

This thesis presents a different approach to the design of smooth developable surfaces with pieces of cones of revolution, which has been introduced by Leopoldseder and Pottmann [22]. The presented algorithms are local and use tools from various branches of classical geometry. In this way one can get valuable insight into the degrees of freedom, the variety of feasible solutions and ways for optimizing them. From now on, these surfaces will be called *cone spline surfaces*. These surfaces are especially useful for applications where the development of the designed surfaces needs to be computed with high accuracy, as numerical integration techniques can be avoided. Furthermore, these surfaces possess the lowest possible parametric and implicit degree for designing G^1 surfaces, their development and bending into other developable shapes is elementary and their offsets are of the same type.

The methods proposed in chapters 1 and 2 for designing cone spline surfaces use known results on *planar and spherical arc splines*. An arc spline is a curve consisting of segments of circles and straight lines that are joined with G^1 continuity. Planar arc spline are desirable paths for numerically controlled cutting machines as their offsets are easy to find. Therefore, there is a rich variety of literature on arc spline approximation of planar curves. A standard method for finding an interpolating arc spline to a planar point set uses biarcs (a biarc is a pair of circular arcs which are tangent continuous at their junction point). One calculates or estimates the tangents at the given points and obtains a one parameter set of biarcs joining these given points and matching the tangents. Different methods for optimizing the free parameter have been proposed and analyzed by Bolton [5], Nutbourne and Martin [30], Piegl [33], Rossignac and Requicha [43], Sabin [44], Schönherr [47], Shippey [51] and Su and Liu [52]. Parkinson and Moreton [31] and Parkinson [32] solve non-linear equations to determine the tangent vectors at the interpolation points such that the arc spline has minimal strain energy. Meek and Walton [26, 27] analyze the resulting errors of the biarc approximation techniques. Furthermore, these authors introduce a different method in [28] to produce an arc spline. They compute a set of osculating circles of a curve and smoothly join consecutive osculating circles by arcs to get a *planar osculating arc spline* approximating the given curve. They show that – asymptotically – this method gives smaller errors than using a biarc spline.

All the contributions on planar biarcs mentioned so far are based on interpolation techniques. Some research on the approximation of planar point sets

has been done by Meek and Walton [25]. Hoschek [15] solves non-linear equation systems to find a least squares fit to such a point set. Wallner [54] uses a generalized multiresolution analysis with trigonometric spline functions in order to approximate a planar curve by an arc spline.

Hoschek and Seemann [14] and Seemann [48] have discussed *spherical* arc spline approximation. Many results on planar arc splines can be applied to spherical arc splines since the planar and spherical case are related via stereographic projection. The approximation of a twisted curve in 3-space with *spatial biarcs* has been analyzed by Fuhs and Stachel [12], Hoschek [15], Nutbourne [30] and Sharrock [50] using geometric methods. Similar to the planar case there is a one parameter set of biarcs joining two points while matching tangents at these points. Seemann [49] uses a different approach to spatial arc splines as he does not interpolate any points but fits a best approximating spatial arc spline to discrete point data by solving a non-linear equation system.

In chapter 3 of this thesis a short introduction to 3-dimensional Euclidean Laguerre geometry is given. In the isotropic model of this geometry an oriented developable surface is just a twisted curve in isotropic 3-space while cones of revolutions appear as isotropic circles. A cone spline surface therefore is transformed to a spatial isotropic arc spline. The cone pair approximation method of developable surfaces presented in chapter 1 in this sense is equivalent to curve approximation with *spatial isotropic biarcs*. The osculating cone splines of chapter 2 lead to *isotropic osculating arc splines*. Both of these methods of curve approximation with isotropic arc splines are analyzed from a geometric point of view.

The great advantage of the interpretation of developable surfaces as isotropic curves with the help of Laguerre geometry lies in the fact that curves are easier to handle than surfaces. With the help of isotropic arc splines a proof is given of the important theorem that two sufficiently close osculating cones of a developable surface can be smoothly joined by a right circular cone segment. This theorem confirms the feasibility and practicality of our osculating cone spline algorithm of chapter 2.

Finally, in chapter 4 of this thesis a geometric method of constructing (Euclidean) *osculating arc splines* is introduced: From a given twisted curve one computes the osculating circles at selected points. Then each two consecutive osculating circles are smoothly joined with an arc which gives a G^1 arc spline. On the one hand this is the adaptation to Euclidean metric of the isotropic osculating arc splines presented in chapter 3, on the other hand it is an extension of the planar osculating arc splines of Meek and Walton [28] to 3-space. Unlike the planar and spherical case where there exists a one parameter set of solution arcs joining two given circles there are, in general, only two complex solution arcs in the 3-dimensional case. Chapter 4 presents a geometric method to find these

solution arcs and proves that to sufficiently close osculating circles of a curve a joining arc exists which is real and useful for applications. Special care has been taken to present a segmentation algorithm of the given curve which is based on geometric properties of the given curve. The practicality of the proposed methods is discussed for several examples.

Chapter 1

Approximation of Developable Surfaces with Cone Pairs

1.1 Fundamentals of developable surfaces

Developable surfaces are surfaces that can be isometrically mapped (*developed*) into the plane. Thus, those surfaces can be unfolded into a plane without stretching or tearing. Assuming sufficient differentiability, they are characterized by the property of possessing vanishing Gaussian curvature. All nonflat developable surfaces are envelopes of one parameter sets of planes. It is a well-known result of differential geometry (see, e.g. [20]) that such a developable surface is either a conical surface, a cylindrical surface, the tangent surface of a twisted curve or a composition of these three surface types. Thus, developable surfaces are ruled surfaces, but with the special property that they possess the same tangent plane at all points of the same generator.

1.1.1 Differential geometric treatment

For an analytical treatment, we will work in the projective extension P^3 of real Euclidean 3-space E^3. We use homogeneous Cartesian coordinates (x_0, x_1, x_2, x_3), collected in the 4-vector $\mathbf{X}$. The one dimensional subspace $\lambda\mathbf{X}$ of $\mathbb{R}^4$ spanned by $\mathbf{X}$ is a point in P^3. This point will also be denoted by $\mathbf{X}$ if no ambiguity can result. For points not at infinity, i.e. $x_0 \neq 0$, the corresponding inhomogeneous Cartesian coordinates are $x = x_1/x_0,\ y = x_2/x_0,\ z = x_3/x_0$; they are comprised in $\mathbf{x} = (x, y, z)$.

The inhomogeneous parametric representation of a ruled surface Γ is

$$\mathbf{g}(u, v) = \mathbf{l}(u) + v\mathbf{e}(u), \tag{1.1}$$

where $\mathbf{l}(u)$ represents a curve on Γ with respect to arc length u and $\mathbf{e}(u)$ are unit vectors of the generator lines. The condition that (1.1) represents a developable surface is

$$\det(\mathbf{l}', \mathbf{e}, \mathbf{e}') = 0 \tag{1.2}$$

with $\mathbf{l}' = d\mathbf{l}/du, \mathbf{e}' = d\mathbf{e}/du$. For a cylinder $\mathbf{e}$ is constant, and for a cone we may choose $\mathbf{l} = const$ as the vertex. In a differential geometric treatment, a tangent surface is written in the form (1.1) with u as arc length of the line of regression $\mathbf{l}$, and $\mathbf{e} = \mathbf{l}'(u)$. Let $\mathbf{e}, \mathbf{p}, \mathbf{n}$ be the Frenet frame vectors of $\mathbf{l}$, with $\mathbf{p}$ and $\mathbf{n}$ as principal normal and binormal, respectively, and let $\varkappa$ and τ be curvature and torsion of $\mathbf{l}$. Then the *Darboux vector*

$$\mathbf{d}(u) = \tau(u)\mathbf{e}(u) + \varkappa(u)\mathbf{n}(u) \tag{1.3}$$

defines the axis $a(u)$: $\mathbf{l}(u) + \lambda\mathbf{d}(u)$ of a cone of revolution $\Delta(u)$ with vertex $\mathbf{l}(u)$, which touches Γ along the generator $e(u)$. Δ is called *osculating cone*, since it has contact of order 2 with Γ at all regular points of the common ruling. This cone may be considered as the counterpart of the osculating circle of a curve; it determines the curvature behavior of a developable surface along a ruling. The conical curvature

$$k(u) = \tau(u)/\varkappa(u) \tag{1.4}$$

is related to the opening angle α of Δ (see Figure 1.2) via $k = cot(\alpha)$ which follows from (1.3).

The rectifying planes $\rho(u) = \mathbf{l}(u) + v_1\mathbf{e}(u) + v_2\mathbf{n}(u)$ of $\mathbf{l}(u)$ envelop another developable surface Γ^*. Its generators are the axes $a(u)$ of $\Delta(u)$ (Figure 1.1). The line of regression of Γ^* is composed of the cuspoidal points

$$\mathbf{m}^*(u) = \mathbf{l}(u) - \frac{\varkappa}{\varkappa\tau' - \varkappa'\tau}(u)\left(\tau(u)\mathbf{e}(u) + \varkappa(u)\mathbf{n}(u)\right) \tag{1.5}$$

on $a(u)$, see e.g. [20]. By using equation (1.4) this can be simplified to

$$\mathbf{m}^*(u) = \mathbf{l}(u) - \frac{1}{k'(u)}\left(k(u)\mathbf{e}(u) + \mathbf{n}(u)\right). \tag{1.6}$$

If a plane ρ rolls on a developable surface Γ^* then a curve e in ρ will trace out a so-called *moulding surface*. Recently, approximation algorithms for moulding surfaces have been proposed in [36]. Figure 1.1 identifies developable surfaces Γ to be special moulding surfaces where the generating curve e is a straight line. During this motion each point $\mathbf{l}(0) + \mu\mathbf{e}(0)$ on e traces out a surface curve

$$\mathbf{o}_\mu(u) = \mathbf{l}(u) + (\mu - u)\mathbf{e}(u), \qquad \mu \in \mathbb{R} \tag{1.7}$$

of Γ. Such a curve intersects all generators of Γ orthogonally as $\mathbf{o}'_\mu \cdot \mathbf{l}' = 0$ is satisfied. These *orthogonal trajectories* of Γ or *filar involutes* of $\mathbf{l}(u)$ are a spatial

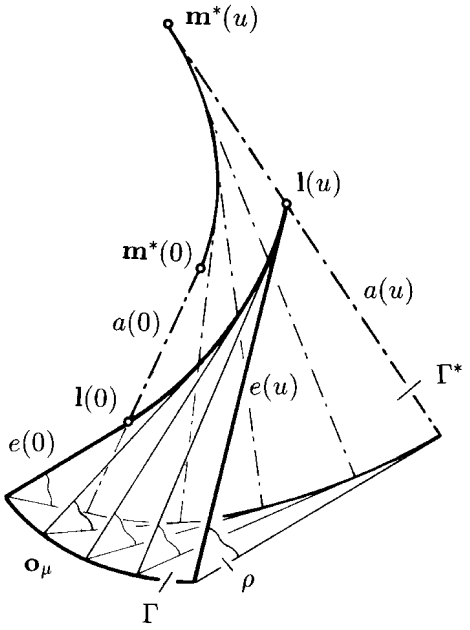

Figure 1.1: Kinematic generation of Γ as a moulding surface

counterpart of involutes of planar curves and form an orthogonal parameter net on Γ together with the generators $e(u)$. For fixed parameter u the osculating circles of $\mathbf{o}_\mu(u), \mu \in \mathbb{R}$ have a common rotation axis and lie on the osculating cone $\Delta(u)$.

We come back to Γ being a conical or cylindrical surface where formula (1.3) is not applicable. If Γ is a general cone with vertex $\mathbf{l}$, the osculating cone Δ contains the osculating circle of the spherical curve $\mathbf{c}(u) = \mathbf{l} + \mathbf{e}(u)$; for a general cylinder, one may compute its intersection curve $\mathbf{c}$ with a plane normal to the generators. Then, the osculating cylinders pass through the osculating circles of $\mathbf{c}$.

The osculating cone or cylinder may degenerate to a plane; the corresponding generator of Γ is then called an *inflection generator*. For a cylinder Γ this happens, if the normal section $\mathbf{c}$ has an inflection point (point with vanishing curvature). A cone Γ has an inflection generator, if the spherical curve $\mathbf{c}$ sends its osculating plane through the vertex. Finally, a tangent surface has an inflection generator if the corresponding point of the line of regression possesses vanishing torsion. For the computation of inflection generators on developable surfaces see for instance [7].

1.1.2 Dual approach to developable surfaces

A plane $u_0 + u_1 x + u_2 y + u_3 z = 0$ can be represented by its homogeneous plane coordinates $\mathbf{U} = (u_0, u_1, u_2, u_3)$. We will also use oriented planes and represent them by normalized plane coordinates, where the normal vector (u_1, u_2, u_3) is normalized, $u_1^2 + u_2^2 + u_3^2 = 1$, and determines the orientation.

The "dual approach" to developable surfaces interprets a *developable NURBS surface* as set of its tangent planes $\mathbf{U}(t)$. It can then be written as

$$\mathbf{U}(t) = \sum_{i=0}^{n} \mathbf{U}_i \, N_i^k(t), \tag{1.8}$$

with the normalized B–spline functions $N_i^k(t)$ of degree k over a given knot vector V. The vectors $\mathbf{U}_i$ are the homogeneous plane coordinate vectors of the *control planes*, also denoted by $\mathbf{U}_i$.

Each generator of the developable surface follows from (1.8) as intersection of the plane $\mathbf{U}(t)$ and its derivative $\dot{\mathbf{U}}(t)$. In particular, the boundary rulings of the surface are the intersections of the boundary control planes $\mathbf{U}_0 \cap \mathbf{U}_1$ and $\mathbf{U}_{n-1} \cap \mathbf{U}_n$. The cuspoidal edge or line of regression is obtained as intersection $\mathbf{U}(t) \cap \dot{\mathbf{U}}(t) \cap \ddot{\mathbf{U}}(t)$. In general, this is a Bézier or B–spline curve of degree $3k - 6$. Recently, algorithms for the computation with the dual representation, the conversion to the standard tensor product representation and the solution of interpolation and approximation algorithms have been developed [17, 18, 37].

For $k = 2$, the developable NURBS surface is composed of pieces of quadratic cones or cylinders. Apart from the polygon connecting the cone vertices, the surface is G^1, i.e. adjacent cones or cylinders are tangent to each other along the common ruling. Even in this simple case, the development of the surface can, in general, not be given in terms of elementary functions. Therefore, we will now study the case where the surface is composed of right circular cones or cylinders only. These surfaces shall be called *cone spline surfaces* henceforth. Figure 1.2 shows the Bézier planes of a right circular cone segment. Using normalized plane coordinates $\mathbf{U}_0$ and $\mathbf{U}_2$, the Bézier plane $\mathbf{U}_1 = (u_{10}, u_{11}, u_{12}, u_{13})$ contains the boundary generators and has the weight

$$w_1 = \sqrt{u_{11}^2 + u_{12}^2 + u_{13}^2} = \frac{\cos\alpha}{\cos\beta},$$

with α and β denoting the angle between the axis a and $\mathbf{U}_0$ or $\mathbf{U}_1$, respectively. It is well known that the point set of such a cone segment could also be represented by a rational Bézier tensor product surface of degree (1,2) (see e.g. [34]).

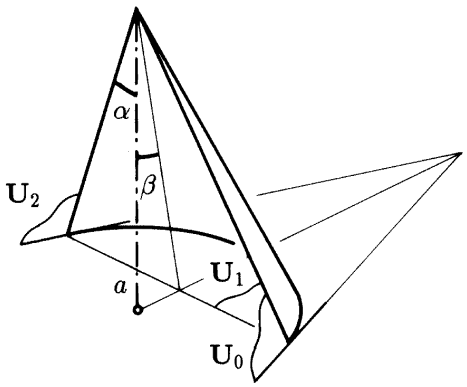

Figure 1.2: Cone segment

1.2 Method

Modeling with cone spline surfaces is thought in the following way. First, the shape of the surface is described in some analytic form, for example (1.8) with arbitrary degree k. Together with this G^1 developable surface Γ we prescribe a region of interest Ω in which Γ is free of singularities. Ω may be a simply connected region, for example a bounding box or a ball, which makes it computationally easy to decide whether or not a point lies in Ω. We would like to approximate Γ by a cone spline surface Λ which is free of singularities inside Ω.

1.2.1 G^1 Hermite elements

The idea is to select a sequence of rulings e_i of Γ, compute their tangent planes τ_i and interpolate consecutive G^1 elements (e_i, τ_i) with two segments of cones of revolution, which possess the same tangent plane along the common generator. Throughout this thesis, we will tacitly allow that the cone may degenerate to a cylinder and mention this case only if necessary. Furthermore, we will simply refer to a segment of a right circular cone, bounded by two generators, as a *cone segment*. The two cone segments which interpolate the given G^1 *Hermite data* form a G^1 *cone pair*. If we want to stress the fact that a cone is not a right circular one we will call it a *general cone*.

For computing a practically useful solution, it is necessary to select special generators of Γ and to introduce some orientations.

Since cones of revolution do not have inflection generators, the typical behavior of an inflection generator can only be represented at a junction of two cones. Therefore, inflection generators should belong to the selected generators. Chalfant and Maekawa [7] introduced a method for computing inflection lines on

developable surfaces. We also propose to select those rulings of the given surface Γ along which we have a G^1 junction of two developable surface patches such that the patches lie locally on different sides of the common tangent plane. If one does not segment at inflection generators our method will produce s-shaped cone pairs, i.e. the cones locally are lying on different sides of the tangent plane at the junction generator. Now, we will focus on the solution of the Hermite interpolation problem.

Let (e_i, τ_i), $i = 1, 2$, be two consecutive G^1 elements. With each element we associate an orthonormal basis $\mathbf{e}_i, \mathbf{p}_i, \mathbf{n}_i$ in the following way (Fig. 1.3). τ_i is

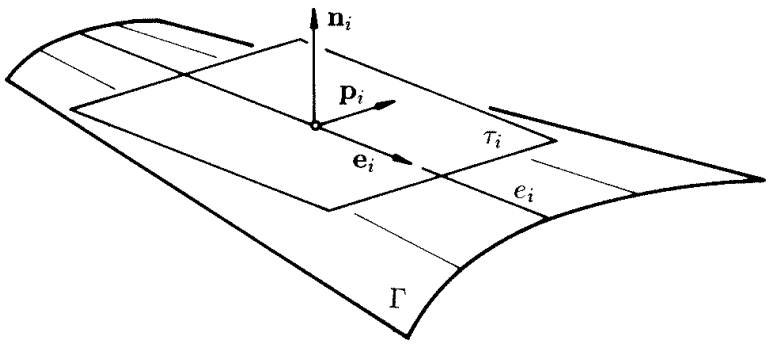

Figure 1.3: Orthonormal basis associated with Hermite element (e_i, τ_i)

spanned by the generator vector $\mathbf{e}_i$ and the unit vector $\mathbf{p}_i$ normal to $\mathbf{e}_i$. The orientation of $\mathbf{e}_i$ is taken from an orientation of the set of generators of the given surface Γ. The vector $\mathbf{p}_i$ indicates the side on which the interpolant between e_i and e_{i+1} has to connect. Thus, the unit normal $\mathbf{n}_i = \mathbf{e}_i \times \mathbf{p}_i$ always points to the same side of the surface Γ, which is assumed to be regular and orientable in the region of interest.

1.2.2 The general case

If two cones of revolution Λ_1, Λ_2 with different vertices $\mathbf{v}_1$, $\mathbf{v}_2$ possess a common generator and tangent plane, their axes either intersect at a point $\mathbf{m}$ or are parallel. We will now treat the first (general) case. Here $\mathbf{m}$ is the center of a sphere Σ that touches both cones along circles c_1, c_2 (Fig. 1.4). Σ can already be computed from the two given G^1 elements. Using a point $\mathbf{l}_i$ on e_i, the midpoint $\mathbf{m}$ of Σ is the intersection of the normal planes

$$\nu_i : \quad (\mathbf{x} - \mathbf{l}_i) \cdot \mathbf{p}_i = 0, \qquad i = 1, 2 \tag{1.9}$$

with the tangent planes' bisector plane

$$\sigma : \quad \mathbf{x} \cdot (\mathbf{n}_1 - \mathbf{n}_2) - \mathbf{l}_1 \cdot \mathbf{n}_1 + \mathbf{l}_2 \cdot \mathbf{n}_2 = 0. \tag{1.10}$$

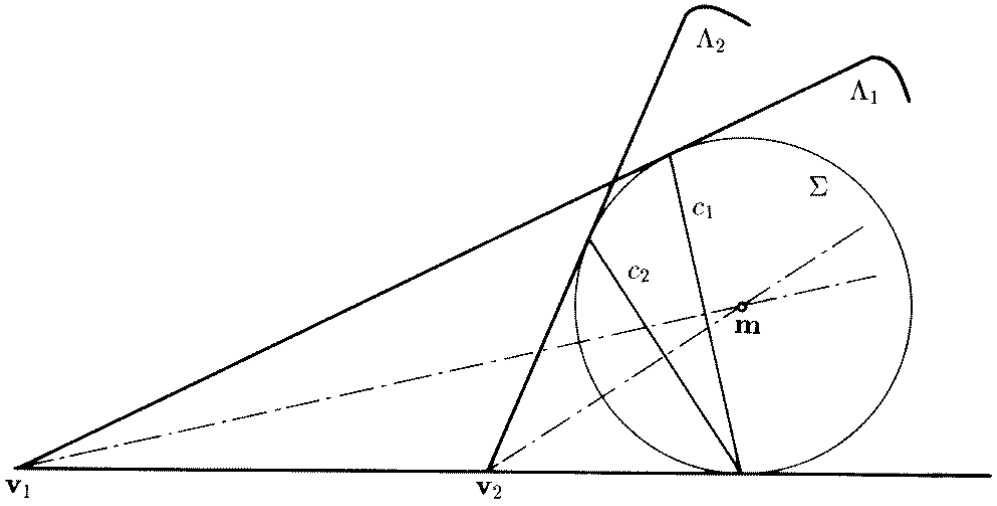

Figure 1.4: Inscribed sphere of two cones

Let $\mathbf{a}_i$ be the touching point of Σ and e_i. The desired cone pair will touch Σ along a G^1 pair of circle segments, i.e. a *spherical biarc*. Its end points are $\mathbf{a}_i$, and the end tangent vectors are $\mathbf{p}_i$. The set of biarcs interpolating two points plus tangent vectors has been studied in [12], [15], [30] or [50] and the results can now be applied to the present problem.

For the rational Bézier representation of the biarc, we denote the Bézier points of its two circle segments c_1, c_2 by $\mathbf{a}_1, \mathbf{b}_1, \mathbf{c}, \mathbf{b}_2, \mathbf{a}_2$ (Fig. 1.5) and let $\mathbf{b}_1 = \mathbf{a}_1 + \lambda_1 \mathbf{p}_1$, $\mathbf{b}_2 = \mathbf{a}_2 - \lambda_2 \mathbf{p}_2$. The two legs in the Bézier polygon of a circle possess equal length

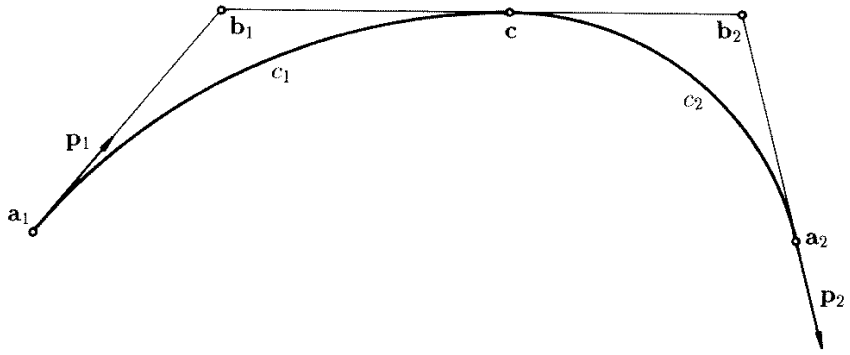

Figure 1.5: Control polygon of a biarc

and thus an admissible pair of inner Bézier points is characterized by

$$(\mathbf{b}_2 - \mathbf{b}_1)^2 = (\lambda_1 + \lambda_2)^2.$$

This is equivalent to

$$(\mathbf{a}_2-\mathbf{a}_1)^2-2\lambda_1(\mathbf{a}_2-\mathbf{a}_1)\cdot\mathbf{p}_1-2\lambda_2(\mathbf{a}_2-\mathbf{a}_1)\cdot\mathbf{p}_2+2\lambda_1\lambda_2(\mathbf{p}_1\cdot\mathbf{p}_2-1)=0. \quad (1.11)$$

We may choose $\mathbf{b}_1(\lambda_1)$ and then compute a unique $\mathbf{b}_2(\lambda_2)$ via (1.11). To complete the rational Bézier representation, we also need the junction point

$$\mathbf{c}=\frac{\lambda_2\mathbf{b}_1+\lambda_1\mathbf{b}_2}{\lambda_1+\lambda_2}. \quad (1.12)$$

Setting the weights at the end points of the two circle segments to 1, the weights w_i at $\mathbf{b}_i$ are computed as

$$|w_i|=\frac{|(\mathbf{b}_i-\mathbf{a}_i)\cdot(\mathbf{c}-\mathbf{a}_i)|}{\|\mathbf{b}_i-\mathbf{a}_i\|\|\mathbf{c}-\mathbf{a}_i\|}.$$

If $\lambda_i>0$, then one uses the arc contained in the triangle $\mathbf{a}_i,\mathbf{b}_i,\mathbf{c}$ and a positive weight w_i. Otherwise one has to use the complementary arc and a negative weight. The homogeneous coordinates of the Bézier points are

$$\mathbf{A}_i=(1,\mathbf{a}_i),\ \mathbf{B}_i=(w_i,w_i\mathbf{b}_i),\ \mathbf{C}=(1,\mathbf{c}).$$

The Bézier planes of the cone segments are the polar planes of these Bézier points with respect to the sphere $\Sigma:(\mathbf{x}-\mathbf{m})^2=r^2$. The homogeneous equation of the polar plane of a point with homogeneous coordinates $\mathbf{Y}=(y_0,\mathbf{y})$ is

$$(\mathbf{x}-x_0\mathbf{m})\cdot(\mathbf{y}-y_0\mathbf{m})=r^2x_0y_0.$$

Clearly, a cone pair and the corresponding spherical biarc are connected via this polarity.

As we have a region Ω of interest, an additional problem has to be considered. For the moment, let us look at a single cone for which we have computed the corresponding spherical arc c with Bézier points $\mathbf{a},\mathbf{b},\mathbf{c}$. As we exclude all solutions with vertex $\mathbf{v}$ in Ω, we have to distinguish between two cases. The first case is shown in Figure 1.6. The sphere Σ and the region Ω lie on the same side of the vertex $\mathbf{v}$. Choosing a point $\mathbf{d}$ of the bounding generator e lying in Ω, this is characterized by

$$(\mathbf{a}-\mathbf{v})\cdot(\mathbf{d}-\mathbf{v})>0.$$

Here c directly corresponds to the useful piece of the cone.

If Σ and Ω lie on different sides of $\mathbf{v}$ however, equivalent to

$$(\mathbf{a}-\mathbf{v})\cdot(\mathbf{d}-\mathbf{v})<0,$$

using the computed arc c would lead to sharp edges in the interpolated surface. Figure 1.7 shows that the arc $\bar{c}$ complementary to c has to be used. This leads

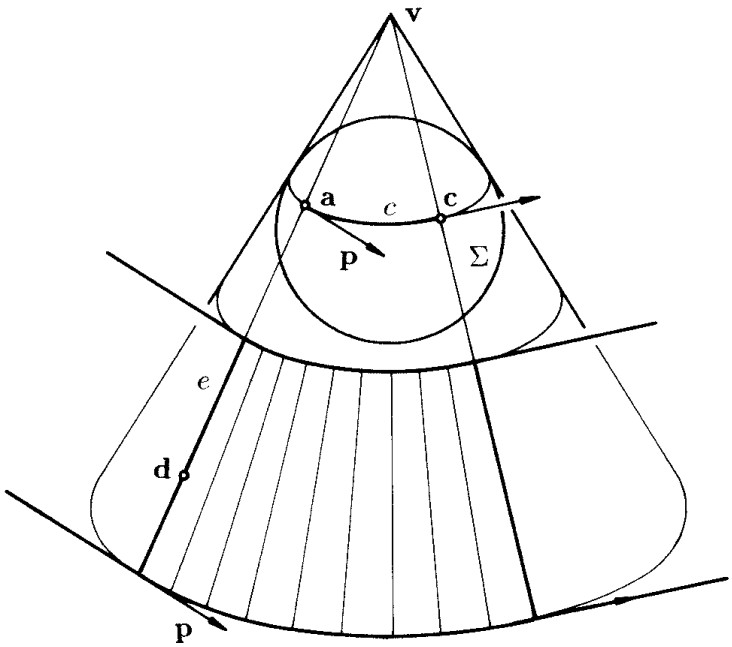

Figure 1.6: Σ and Ω lying on the same side of $\mathbf{v}$

to sharp edges in the spherical arc spline on Σ, but guarantees a smooth surface. The change from c to $\bar{c}$ is easily accomplished by changing the sign of the weight w of the inner Bézier point $\mathbf{B} = (w, w\mathbf{b})$.

The vertices $\mathbf{v}_i$ of the two cone segments can be computed by intersecting the tangent plane of Σ at $\mathbf{c}$ with the boundary generators e_i. We can also first compute the vertices in a way analogous to the inner Bézier points. Letting $\mathbf{v}_1 = \mathbf{a}_1 + \mu_1\mathbf{e}_1$, $\mathbf{v}_2 = \mathbf{a}_2 - \mu_2\mathbf{e}_2$, an admissible vertex pair is characterized by

$$(\mathbf{v}_2 - \mathbf{v}_1)^2 = (\mu_1 + \mu_2)^2.$$

Similar to (1.11), this yields a bilinear relation between μ_1, μ_2, given by

$$(\mathbf{a}_2 - \mathbf{a}_1)^2 - 2\mu_1(\mathbf{a}_2 - \mathbf{a}_1)\cdot\mathbf{e}_1 - 2\mu_2(\mathbf{a}_2 - \mathbf{a}_1)\cdot\mathbf{e}_2 + 2\mu_1\mu_2(\mathbf{e}_1\cdot\mathbf{e}_2 - 1) = 0. \quad (1.13)$$

In order to determine a cone pair within the one parameter set of solutions we can either choose $\mathbf{b}_1(\lambda_1)$ and compute $\mathbf{b}_2(\lambda_2)$ or choose $\mathbf{v}_1(\mu_1)$ and compute $\mathbf{v}_2(\mu_2)$. We see that both mappings $\mathbf{b}_1 \mapsto \mathbf{b}_2$ and $\mathbf{v}_1 \mapsto \mathbf{v}_2$ are projective maps. The connecting rulings $\mathbf{v}_1\mathbf{v}_2$ therefore lie in a ruled quadric Φ. According to Fuhs and Stachel [12], Φ is a hyperboloid of revolution, which touches the sphere Σ along a circle, which the connecting points $\mathbf{c}$ of the spherical biarcs are lying on (Fig. 1.8). The tangent planes of Σ (and Φ) along the circle c are the tangent planes of the cone pairs at their junction generators; they envelope a cone of revolution. Discussing degeneracies and special cases later, we summarize:

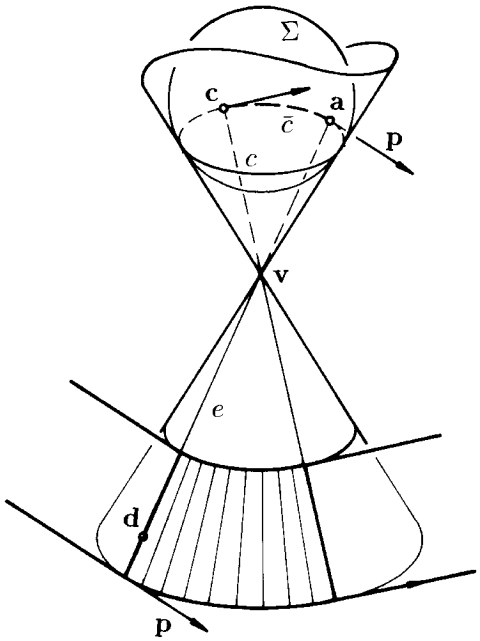

Figure 1.7: Σ and Ω lying on different sides of $\mathbf{v}$

Theorem 1.1 *Given two G^1 elements (e_i, τ_i) in general position, there is a one parameter family of cone pairs interpolating these data. The cones possess a common inscribed sphere Σ. The junction generators of the cone pairs form a set of rulings on a hyperboloid of revolution Φ, which touches Σ along a circle. The generators e_1, e_2 lie in the second set of rulings of Φ. The tangent planes of Σ and Φ along this circle are the junction tangent planes of the cone pairs.*

Let us now discuss some special solutions within the one parameter family we have obtained so far.

In case that the surface to be approximated possesses a generator e_i whose singular point is at infinity, we might want to find a solution in which vertex $\mathbf{v}_i$ of the cone pair is at infinity and thus the first of the two cone segments is a *cylindrical segment*. In view of (1.13) this occurs if

$$\mu_2 = \frac{(\mathbf{a}_2 - \mathbf{a}_1) \cdot \mathbf{e}_1}{\mathbf{e}_1 \cdot \mathbf{e}_2 - 1}. \tag{1.14}$$

The cones which the two segments of a pair are taken from are *congruent*, if $\mu_1 = \mu_2$. Hence, these cone pairs belong to solutions of the quadratic equation, which arises from (1.13) with $\mu_1 = \mu_2$. It always has two real solutions, which is in accordance with a result by Fuhs and Stachel [12] on spherical biarcs consisting of circles of equal radius.

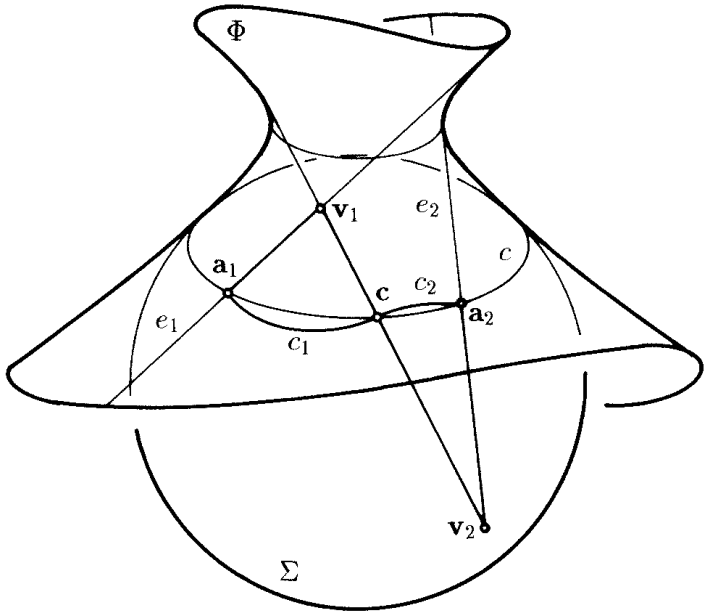

Figure 1.8: Spherical biarc

As practically useful cone pairs one can identify those with (locally) *minimal vertex distance* $\|\Delta\mathbf{v}\| = \|\mathbf{v}_2 - \mathbf{v}_1\| = |\mu_1 + \mu_2|$ (see section 1.4). Writing equation (1.13) in the form

$$\mu_2 = \frac{A\mu_1 + B}{C\mu_1 + D}, \tag{1.15}$$

this cone pair belongs to a solution of

$$C^2\mu_1^2 + 2CD\mu_1 + AD + D^2 - BC = 0. \tag{1.16}$$

Figure 1.9 shows a typical function $\|\Delta\mathbf{v}(\mu_1)\|$ taken from the example in Fig-

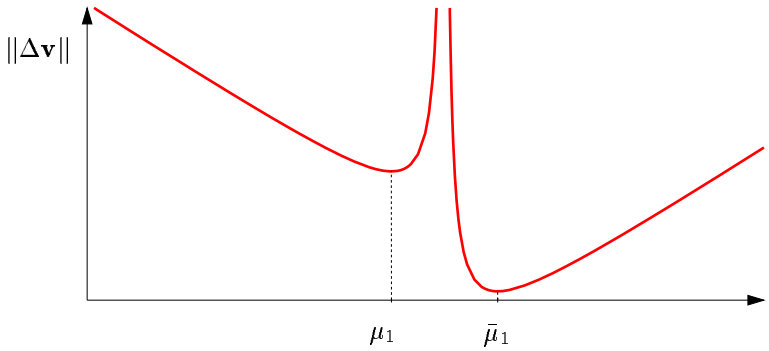

Figure 1.9: Vertex distance function

ure 1.13. One has to take attention that only one of the two solutions μ_1, $\bar{\mu}_1$

leads to a cone pair useful for applications. In section 1.4 it will be shown that in general the practical solution corresponds to the local minimum μ_1 that is *not* the global minimum. In the example of Figure 1.9 the global minimum $\bar{\mu}_1$ would produce a loop in the cone spline surface.

Equation (1.16) always has two real solutions: According to Theorem 1.1, we have to find those rulings of the hyperboloid Φ, which intersect the generators e_i in points $\mathbf{v}_i$ with minimal distance from each other. Using the top view of Φ, the images of all rulings of Φ are tangent to the circular silhouette u' of Φ. As all rulings of Φ are constantly sloped, one only has to find those with minimal distance $\mathbf{v}_1'\mathbf{v}_2'$ (Fig. 1.10). These special solutions of junction generators $\mathbf{v}_1\mathbf{v}_2$ can

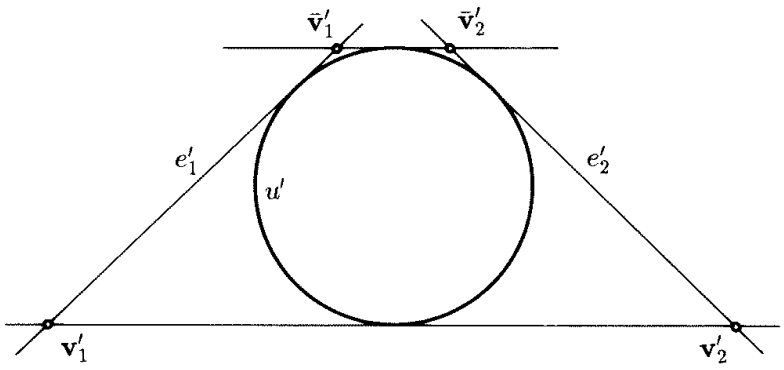

Figure 1.10: Minimal vertex distance $\mathbf{v}_1\mathbf{v}_2$

also be characterized by the fact that the generator $\mathbf{v}_1\mathbf{v}_2$ defines the same angle with both generators e_i.

Nutbourne and Martin [30] have shown how to minimize the angle between the planes of c_1 and c_2. This can be achieved by minimizing the distance $\|\mathbf{b}_2 - \mathbf{b}_1\| = |\lambda_1 + \lambda_2|$ of the control points $\mathbf{b}_i$ in Figure 1.5. Additionally, the winding angles of c_1 and c_2 are equal then.

1.2.3 Special cases

Important special cases arise if the developable surface Γ to be approximated (locally) is a general cone, a general cylinder or a surface of constant slope, that is the tangent surface of a curve whose tangent vectors enclose a constant angle with some plane π (Fig. 1.11). Any osculating cone Δ_i of a developable surface of constant slope has its axis normal to π. For any two tangent planes $\tau_i, i = 1, 2$ touching Γ along e_i we have $\mathbf{p}_i$ parallel to π and the normal vectors $\mathbf{n}_i$ enclose a constant angle with π.

In the following we look at two consecutive G^1 elements $(e_i, \tau_i), i = 1, 2$. Using these data only, we characterize the special cases and derive algorithms to

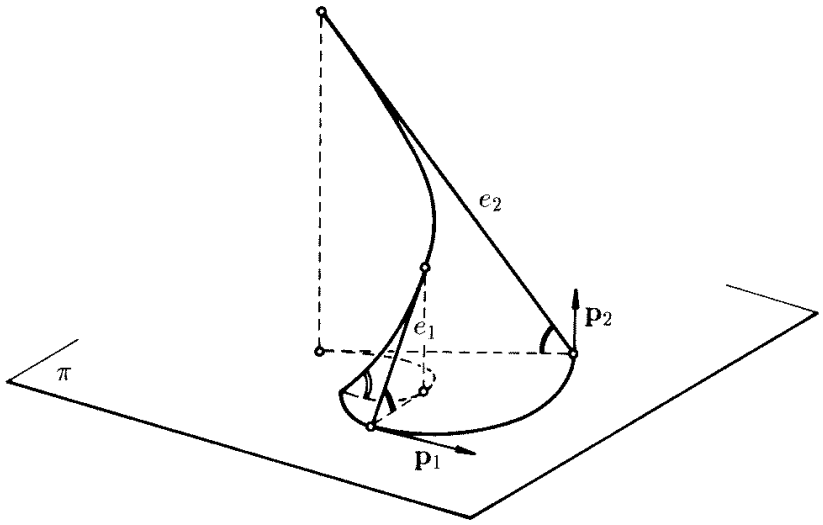

Figure 1.11: Surface of constant slope

interpolate the given boundary elements with a pair of cone or cylinder segments. These algorithms will prove to be similar to the general case discussed in the previous section.

The cone case

The generators e_1, e_2 intersect in a point $\mathbf{v}$. If additionally $\tau_1 = \tau_2$, we interpolate with a part of τ_1. Otherwise, two cone segments with common vertex $\mathbf{v}$ will be used which intersect a sphere Σ centered in $\mathbf{v}$ in a spherical biarc. The one parameter set of solutions is determined by the end points $\mathbf{a}_i = e_i \cap \Sigma$ and end tangent vectors $\mathbf{p}_i$. The missing Bézier points $\mathbf{b}_1 = \mathbf{a}_1 + \lambda_1 \mathbf{p}_1, \mathbf{c}, \mathbf{b}_2 = \mathbf{a}_2 - \lambda_2 \mathbf{p}_2$ can be computed using formulae (1.11) and (1.12).

The cylinder case

The generators e_1, e_2 are parallel and have the same orientation. This case is similar to the first one, with $\mathbf{v}$ being a point at infinity. We interpolate with a planar surface in case of $\tau_1 = \tau_2$, otherwise with a pair of right orthogonal cylinder segments. Intersecting (e_i, τ_i) with a plane normal to e_i we get Hermite elements $(\mathbf{a}_i, \mathbf{p}_i)$ that can be interpolated by a one parameter set of planar biarcs. Obviously (1.11) and (1.12) can also be used for calculating the inner Bézier points of planar biarcs.

Surfaces of constant slope

In the following the generators e_1, e_2 have no point in common.

Given two G^1 Hermite elements in general position we found the center m of a common inscribed sphere as intersection of three planes which had normal vectors $\mathbf{p}_1, \mathbf{p}_2$ and $\mathbf{n}_1 - \mathbf{n}_2$, according to equations (1.9) and (1.10). This calculation is not possible if

$$\det(\mathbf{p}_1, \mathbf{p}_2, \mathbf{n}_1 - \mathbf{n}_2) = 0, \tag{1.17}$$

i.e., the three planes do not intersect in a point. Equation (1.17) is equivalent to

$$(\mathbf{p}_1 \times \mathbf{p}_2) \cdot \mathbf{n}_1 = (\mathbf{p}_1 \times \mathbf{p}_2) \cdot \mathbf{n}_2.$$

Assuming $\det(\mathbf{p}_1, \mathbf{p}_2) \neq 0$ for the moment, the normal vectors $\mathbf{n}_1, \mathbf{n}_2$ enclose the same angle with a plane π spanned by $\mathbf{p}_1$ and $\mathbf{p}_2$. We will now interpolate the given boundary generators by a cone pair with parallel axes, both being normal to π. The cone pair intersects π in a planar biarc (Fig. 1.12) with $\mathbf{a}_i = e_i \cap \pi$ as end points and tangent vectors $\mathbf{p}_i$. Admissible Bézier points $\mathbf{b}_1, \mathbf{c}, \mathbf{b}_2$ again follow

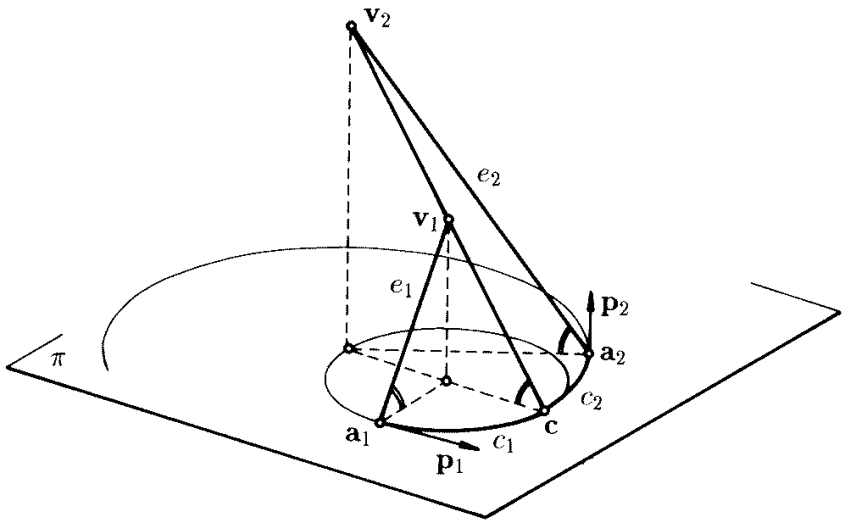

Figure 1.12: Pair of cone segments

from (1.11) and (1.12). The vertices $\mathbf{v}_1$ and $\mathbf{v}_2$ are the intersection points of the generators e_1 and e_2 with $\nu: \ (\mathbf{x} - \mathbf{c}) \cdot (\mathbf{b}_2 - \mathbf{b}_1) = 0$, which is the plane through the junction point $\mathbf{c}$ perpendicular to the junction tangent in $\mathbf{c}$. One can also compute the vertices directly, using $\mathbf{v}_1 = \mathbf{a}_1 + \mu_1 \mathbf{e}_1, \mathbf{v}_2 = \mathbf{a}_2 - \mu_2 \mathbf{e}_2$ and equation (1.13). Minimizing the vertex distance with formula (1.16) provides congruent cone segments.

In the case of $\det(\mathbf{p}_1, \mathbf{p}_2) = 0$, which was excluded above, the plane π has to be spanned by $\mathbf{p}_1$ and $\mathbf{n}_1 - \mathbf{n}_2$. The remaining algorithms stay the same.

1.3 Examples

The first example shall demonstrate the general case. Figure 1.13(a) shows a tangent surface Γ. Using four Hermite elements (e_i, τ_i) of Γ as input data we get

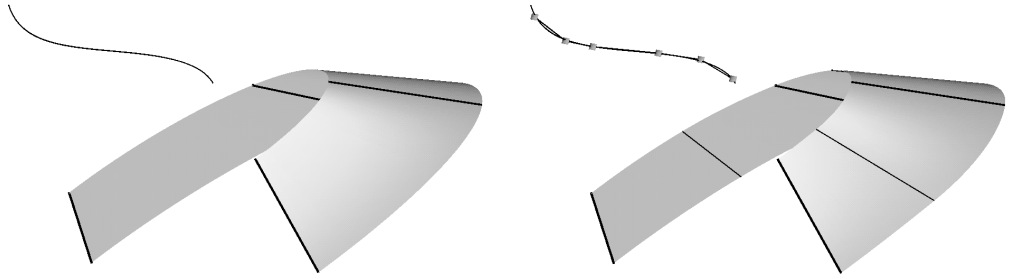

(a) (b)

Figure 1.13: (a) Tangent surface, (b) its approximation with 3 cone pairs

an approximation by three cone pairs, see Figure 1.13(b). From the one parameter set of solutions those with minimal vertex distance are chosen. Connecting the six vertices of the cone segments to a polygon we obtain the locus of all the singular points of the cone spline surface. Although the line of regression was not used in the computation of the cone spline, one can see that this curve is approximated perfectly by the vertex polygon.

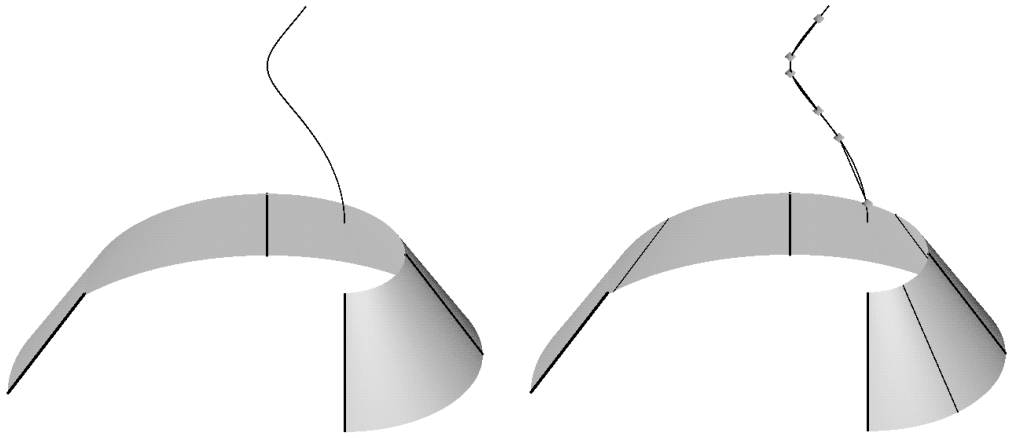

(a) (b)

Figure 1.14: (a) Surface of constant slope, (b) its approximation with 3 cone pairs

The second example illustrates one of our special cases and shows the approximation of the tangent surface of a helical curve (Fig. 1.14). The approximation

of this surface of constant slope with only a small number of cone segments is again very good.

1.4 Approximation quality

Let the given developable surface Γ be the tangent surface of a twisted curve $\mathbf{l}(u)$ which is sufficiently differentiable. Let u denote its arc length, $\varkappa(u)$ and $\tau(u)$ its curvature and torsion. After choosing two Hermite elements $(e_i, \tau_i), i = 1, 2$ of Γ our algorithm is based on a sphere Σ which touches both Hermite elements. On Σ we obtain biarcs which correspond to cone pairs joining the Hermite elements. We now want to analyze our algorithm for Hermite elements (e_i, τ_i) which lie 'close' to each other.

By using the Taylor expansion of the line of regression $\mathbf{l}(u)$ at the point $\mathbf{l}(0)$ we will look into the limit case of joining Hermite elements $(e(0), \tau(0))$ and $(e(u), \tau(u))$ for $u \to 0$. The spheres $\Sigma(u)$ touching these Hermite elements will turn out to converge to a limit sphere which does not possess vanishing radius. A geometric interpretation of this limit sphere will be given.

There is a one parameter set of cone pairs joining the Hermite elements $(e(0), \tau(0))$ and $(e(u), \tau(u))$. In section 1.2.2 we proposed to minimize the distance of the cone vertices. The feasibility of this choice of the free parameter will be derived from the following calculations.

The Taylor expansion of the line of regression $\mathbf{l}(u)$ of Γ at the point $\mathbf{l}(0)$ is

$$\mathbf{l}(u) = \mathbf{l}(0) + \mathbf{l}'(0)u + \frac{\mathbf{l}''(0)}{2!}u^2 + \frac{\mathbf{l}^{(3)}(0)}{3!}u^3 + \frac{\mathbf{l}^{(4)}(0)}{4!}u^4 + O(u^5). \tag{1.18}$$

Denoting tangent vector, principal normal vector and binormal vector in $\mathbf{l}(0)$ with $\mathbf{e} = \mathbf{e}(0)$, $\mathbf{p} = \mathbf{p}(0)$, $\mathbf{n} = \mathbf{n}(0)$ and employing the Frenet formulae for spatial curves the derivatives of $\mathbf{l}(u)$ with respect to arc length u are given by

$$\begin{aligned}
\mathbf{l}'(0) &= \mathbf{e}, \\
\mathbf{l}''(0) &= \varkappa\mathbf{p}, \\
\mathbf{l}^{(3)}(0) &= -\varkappa^2\mathbf{e} + \varkappa'\mathbf{p} + \varkappa\tau\mathbf{n}, \\
\mathbf{l}^{(4)}(0) &= -3\varkappa\varkappa'\mathbf{e} + (\varkappa'' - \varkappa^3 - \varkappa\tau^2)\mathbf{p} + (2\varkappa'\tau + \varkappa\tau')\mathbf{n}, \\
&\dots
\end{aligned} \tag{1.19}$$

where $\varkappa = \varkappa(0)$ and $\tau = \tau(0)$ are curvature and torsion at $\mathbf{l}(0)$ and $\varkappa' = (d\varkappa/du)(0)$, $\varkappa'' = (d^2\varkappa/du^2)(0)$, $\tau' = (d\tau/du)(0)$, ... the derivatives of $\varkappa(u)$ and $\tau(u)$ with respect to arc length in $\mathbf{l}(0)$. With $\mathbf{l}(0)$ as origin and the Frenet

vectors $\mathbf{e}, \mathbf{p}, \mathbf{n}$ as axes of a coordinate system (1.18) and (1.19) give

$$\mathbf{l}(u) = \begin{pmatrix} u & - & \varkappa^2\frac{u^3}{3!} & - & 3\varkappa\varkappa'\frac{u^4}{4!} & + & O(u^5) \\ & \varkappa\frac{u^2}{2!} + & \varkappa'\frac{u^3}{3!} & + & (\varkappa'' - \varkappa^3 - \varkappa\tau^2)\frac{u^4}{4!} & + & O(u^5) \\ & & \varkappa\tau\frac{u^3}{3!} & + & (2\varkappa'\tau + \varkappa\tau')\frac{u^4}{4!} & + & O(u^5) \end{pmatrix}. \tag{1.20}$$

The tangent vector

$$\mathbf{l}'(u) = \begin{pmatrix} 1 & - & \varkappa^2\frac{u^2}{2!} & - & 3\varkappa\varkappa'\frac{u^3}{3!} & + & O(u^4) \\ & \varkappa u + & \varkappa'\frac{u^2}{2!} & + & (\varkappa'' - \varkappa^3 - \varkappa\tau^2)\frac{u^3}{3!} & + & O(u^4) \\ & & \varkappa\tau\frac{u^2}{2!} & + & (2\varkappa'\tau + \varkappa\tau')\frac{u^3}{3!} & + & O(u^4) \end{pmatrix} \tag{1.21}$$

denotes the direction of the generator $e(u)$ of Γ. The normal vector of the tangent plane $\tau(u)$ along $e(u)$ is given by

$$\mathbf{n}(u) = \frac{\mathbf{l}'(u) \times \mathbf{l}''(u)}{||\mathbf{l}'(u) \times \mathbf{l}''(u)||} \tag{1.22}$$

which leads to

$$\mathbf{n}(u) = \begin{pmatrix} & & \varkappa\tau\frac{u^2}{2!} & + & (2\varkappa\tau' + \tau\varkappa')\frac{u^3}{3!} & + & O(u^4) \\ & -\tau u - & \tau'\frac{u^2}{2!} & + & (-\tau'' + \tau\varkappa^2 + \tau^3)\frac{u^3}{3!} & + & O(u^4) \\ 1 & - & \tau^2\frac{u^2}{2!} & - & 3\tau\tau'\frac{u^3}{3!} & + & O(u^4) \end{pmatrix}. \tag{1.23}$$

We will now use these equations to join the Hermite elements $(e(0), \tau(0))$ and $(e(u), \tau(u))$ by a cone pair. Initially we compute the sphere $\Sigma(u)$ which touches both Hermite elements. The center $\mathbf{m}(u)$ can be found as intersection of three planes according to equations (1.9) and (1.10). Inserting (1.4), (1.21) and (1.23) one obtains

$$\mathbf{m}(u) = \begin{pmatrix} -\frac{k}{k'} & + & \frac{kk''}{2k'^2}u & + & O(u^2) \\ & & 0 & & \\ -\frac{1}{k'} & + & \frac{k''}{2k'^2}u & + & O(u^2) \end{pmatrix}. \tag{1.24}$$

The third coordinate of $\mathbf{m}(u)$ denotes the distance to generator $e(0)$ and is therefore the radius

$$r(u) = -\frac{1}{k'} + \frac{k''}{2k'^2}u + O(u^2) \tag{1.25}$$

of the sphere $\Sigma(u)$. With $\mathbf{m}^*(u)$ from formula (1.6) and its derivative

$$(\mathbf{m}^*)'(u) = \frac{kk''}{k'^2}(u)\mathbf{e}(u) + \frac{k''}{k'^2}(u)\mathbf{n}(u)$$

(1.24) simplifies to

$$\mathbf{m}(u) = \mathbf{m}^*(0) + \frac{1}{2}(\mathbf{m}^*)'(0)u + O(u^2). \tag{1.26}$$

Thus, in the first order approximation the midpoint $\mathbf{m}$ of Σ lies halfway between $\mathbf{m}^*(0)$ and $\mathbf{m}^*(u) = \mathbf{m}^*(0) + (\mathbf{m}^*)'(0)u + O(u^2)$. The geometric interpretation of this property is illustrated in Fig. 1.15: Similar to the kinematic generation

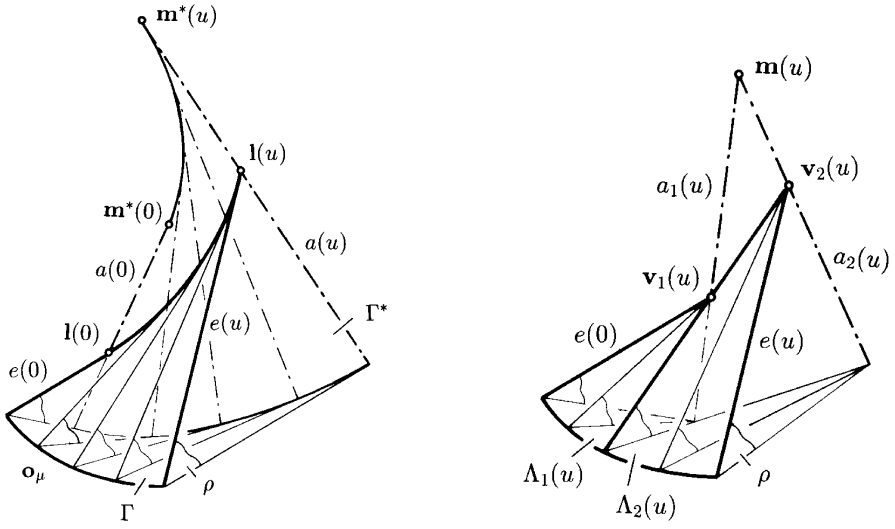

Figure 1.15: Kinematic generation of (a) a developable surface and (b) an approximating cone pair

of a developable surface as a moulding surface (Fig. 1.15(a), see section 1.1.1) one can give a kinematic generation of its cone pair approximation. Let a plane ρ rotate around two intersecting axes a_1 and a_2 as in Figure 1.15(b). Then a line e in ρ will trace out a cone pair. Comparing Fig. 1.15(a) and (b), the set of Darboux axes $a(u)$ of Γ is replaced by two rotation axes $a_1(u)$ and $a_2(u)$ which intersect in the midpoint $\mathbf{m}(u)$ of $\Sigma(u)$ (see Figure 1.4). Formula (1.26) reveals this geometric property.

Let us assume fixed parameter value u for the moment. $\Sigma(u)$ and its midpoint $\mathbf{m}(u)$ are uniquely determined by the Hermite elements $(e(0), \tau(0))$, $(e(u), \tau(u))$. There is still a free parameter for the choice of cone pairs $\Lambda_1(u)$, $\Lambda_2(u)$ which will be eliminated by minimizing the vertex distance $\|\mathbf{v}_2(u) - \mathbf{v}_1(u)\|$. Then, the vertices $\mathbf{v}_1(u)$ on $e_1 := e(0)$ and $\mathbf{v}_2(u)$ on $e_2 := e(u)$ merely depend on u. For the computation of the vertices $\mathbf{v}_1(u), \mathbf{v}_2(u)$ we follow the course of section 1.2.2. One will expect $\mathbf{v}_1(u)$, $\mathbf{v}_2(u)$ to approximate $\mathbf{l}(0)$, $\mathbf{l}(u)$ as the vertex polygon of the cone spline surface shall approximate the line of regression.

First we need to calculate the points $\mathbf{a}_1(u)$ and $\mathbf{a}_2(u)$ where $\Sigma(u)$ touches $e_1 = e(0)$ and $e_2 = e(u)$ (see Figure 1.16 for $\mathbf{a}_1(u)$). With (1.24) the parameter

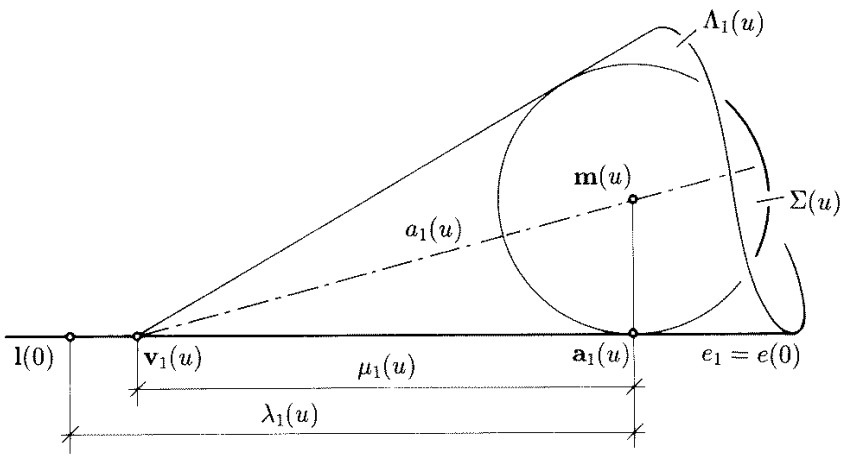

Figure 1.16: Sphere $\Sigma(u)$ touching $(e(0), \tau(0))$

$\lambda_1(u)$ in $\mathbf{a}_1(u) = \mathbf{l}(0) + \lambda_1(u)\mathbf{l}'(0)$ equals

$$\lambda_1(u) = -\frac{k}{k'} + \frac{kk''}{2k'^2}u + O(u^2) \tag{1.27}$$

and this leads to

$$\mathbf{a}_1(u) = \begin{pmatrix} -\frac{k}{k'} & + & \frac{kk''}{2k'^2}u & + & O(u^2) \\ & & 0 & & \\ & & 0 & & \end{pmatrix}. \tag{1.28}$$

The second generator $e(u)$ is touched by $\Sigma(u)$ in $\mathbf{a}_2(u) = \mathbf{l}(u) + \lambda_2(u)\mathbf{l}'(u)$ to parameter

$$\lambda_2(u) = (\mathbf{m}(u) - \mathbf{l}(u)) \cdot \mathbf{l}'(u).$$

With (1.20), (1.21) and (1.24) this simplifies to

$$\lambda_2(u) = -\frac{k}{k'} + (\frac{kk''}{2k'^2} - 1)u + O(u^2) \tag{1.29}$$

and gives

$$\mathbf{a}_2(u) = \begin{pmatrix} -\frac{k}{k'} & + & \frac{kk''}{2k'^2}u & + & O(u^2) \\ & - & \frac{\tau}{k'}u & + & O(u^2) \\ & & & & O(u^2) \end{pmatrix}. \tag{1.30}$$

A possible vertex pair $\mathbf{v}_1(u) = \mathbf{a}_1(u) + \mu_1(u)\mathbf{e}_1(u)$, $\mathbf{v}_2(u) = \mathbf{a}_2(u) - \mu_2(u)\mathbf{e}_2(u)$ where $\mathbf{e}_1(u) = \mathbf{l}'(0)$, $\mathbf{e}_2(u) = \mathbf{l}'(u)$ has to fulfill the bilinear relation (1.13) for

$\mu_1(u), \mu_2(u)$. For the minimization of the vertex distance $\|\mathbf{v}_2(u) - \mathbf{v}_1(u)\|$ one has to solve the quadratic equation (1.16). Inserting (1.28) and (1.30) one obtains the two solutions

$$\begin{aligned} \mu_1(u) &= -\tfrac{k}{k'} + (\tfrac{kk''}{2k'^2} + \tfrac{1}{3} - \tfrac{1}{6})u + O(u^2), \\ \bar{\mu}_1(u) &= -\tfrac{k}{k'} + (\tfrac{kk''}{2k'^2} + \tfrac{1}{3} + \tfrac{1}{6})u + O(u^2). \end{aligned} \tag{1.31}$$

Note, that one has to evaluate (1.28) and (1.30) up to third order in u to obtain (1.31).

In the following we will identify $\mu_1(u)$ of (1.31) as the useful solution while $\bar{\mu}_1(u)$ will not lead to a practically useful cone pair. Let us analyze the good solution first. With (1.27) and (1.31) the vertex $\mathbf{v}_1(u) = \mathbf{a}_1(u) + \mu_1(u)\mathbf{l}'(0) = \mathbf{l}(0) + (\lambda_1 + \mu_1)\mathbf{l}'(0)$ simplifies to

$$\mathbf{v}_1(u) = \mathbf{l}(0) + (\frac{1}{6}u + O(u^2))\mathbf{l}'(0). \tag{1.32}$$

Similarly the vertex $\mathbf{v}_2(u)$ of $\Lambda_2(u)$ equals

$$\mathbf{v}_2(u) = \mathbf{l}(u) - (\frac{1}{6}u + O(u^2))\mathbf{l}'(u). \tag{1.33}$$

The vector $\Delta\mathbf{v}(u) = \mathbf{v}_2(u) - \mathbf{v}_1(u)$ (Fig. 1.17) which gives the direction of the

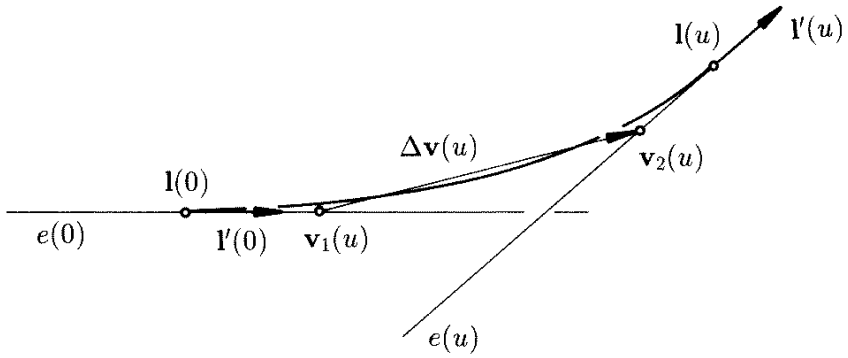

Figure 1.17: Line of regression $\mathbf{l}(u)$ with approximating vertex polygon

common generator $\mathbf{v}_1(u)\mathbf{v}_2(u)$ of $\Lambda_1(u)$ and $\Lambda_2(u)$ simplifies to

$$\Delta\mathbf{v}(u) = \frac{2}{3}u \begin{pmatrix} 1 & + & O(u^2) \\ \frac{\varkappa}{2}u & + & O(u^2) \\ & & O(u^2) \end{pmatrix}. \tag{1.34}$$

Thus, the junction generator $\mathbf{v}_1\mathbf{v}_2$ approximates the generator $e(u/2)$: $\mathbf{l}(u/2) + \lambda\mathbf{l}'(u/2)$ of Γ, since

$$\mathbf{l}'(u/2) = \begin{pmatrix} 1 & + & O(u^2) \\ \frac{\varkappa}{2}u & + & O(u^2) \\ & & O(u^2) \end{pmatrix}.$$

Equations (1.32) and (1.33) give

$$\|\mathbf{v}_1(u) - \mathbf{l}(0)\| = \|\mathbf{v}_2(u) - \mathbf{l}(u)\| = \frac{1}{6}u + O(u^2)$$

which, according to (1.34), asymptotically equals a quarter of the vertex distance

$$\|\mathbf{v}_2(u) - \mathbf{v}_1(u)\| = \frac{2}{3}u + O(u^2).$$

This shows that a cone spline surface generated with the cone pair algorithm possesses a vertex polygon $\mathbf{v}_1, \mathbf{v}_2, \mathbf{v}_3, \ldots$ such that asymptotically

$$\|\mathbf{v}_2 - \mathbf{v}_1\| + \|\mathbf{v}_4 - \mathbf{v}_3\| + \cdots = 2\left(\|\mathbf{v}_1 - \mathbf{l}(0)\| + \|\mathbf{v}_3 - \mathbf{v}_2\| + \|\mathbf{v}_5 - \mathbf{v}_4\| + \cdots\right)$$

holds true. This uneven distribution of the vertices can be noticed in all the examples given in Figures 1.13, 1.14 and 2.8.

Finally, let us focus on the second solution $\bar{\mu}_1(u)$ of (1.31). Completely similar to the calculations above we obtain vertices

$$\begin{aligned} \bar{\mathbf{v}}_1(u) &= \mathbf{l}(0) + (\tfrac{1}{2}u + O(u^2))\mathbf{l}'(0), \\ \bar{\mathbf{v}}_2(u) &= \mathbf{l}(u) - (\tfrac{1}{2}u + O(u^2))\mathbf{l}'(u). \end{aligned}$$

The vector

$$\Delta\bar{\mathbf{v}}(u) = \bar{\mathbf{v}}_2(u) - \bar{\mathbf{v}}_1(u) = \frac{1}{12}u^3 \begin{pmatrix} \varkappa^2 & + & O(u) \\ \varkappa' & + & O(u) \\ \varkappa\tau & + & O(u) \end{pmatrix}$$

does not approximate the direction of a generator e of Γ. The resulting cone pair is not practical for the approximation of Γ. The length of $\Delta\bar{\mathbf{v}}(u)$ is of third order in u in contrast with the length of $\Delta\mathbf{v}(u)$ in (1.34) which is of first order in u. Thus the solution $\bar{\mu}_1$ will — for sufficiently small u — lead to the *global* minimum of the vertex distance function.

Chapter 2

Osculating Cone Splines

2.1 Method

Recently, Meek and Walton [28] have studied the approximation of plane curves with *osculating arc splines*. These are circular splines which contain a sequence of segments of osculating circles of the curve to be approximated. Between two consecutive osculating circles one circle segment is built in. It has been shown that the method results in curves with a smaller error than those produced from biarcs [27, 28].

We will now investigate the analogue for cone spline surfaces. Given a developable surface Γ that is neither a general cone or cylinder nor a surface of constant slope, we compute a sequence of osculating cones Δ_i and smoothly join consecutive cones by a cone Δ. The special cases excluded above will be treated in section 2.1.1.

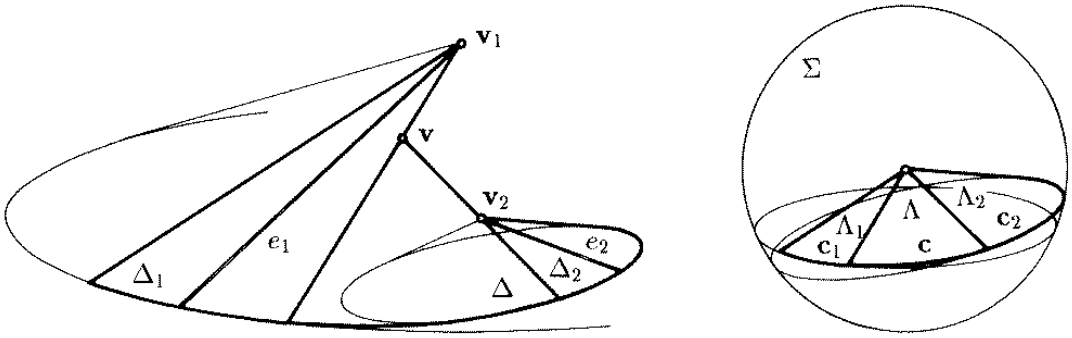

Figure 2.1: Joining cones Δ_i and Λ_i

Let us assume that Δ_1, Δ_2 are not cylinders. If a cone Δ smoothly joins these two cones, we may perform translations which take their vertices to the origin.

The resulting three cones $\Lambda_1, \Lambda, \Lambda_2$ are again smoothly joined. The relevant segments intersect the unit sphere Σ in a spherical triarc, formed by segments of circles $\mathbf{c}_1, \mathbf{c}, \mathbf{c}_2$ (Fig. 2.1). Thus, we will first focus on the problem of finding a joining arc c to two given arcs c_1, c_2 on a sphere Σ.

From the given cones Δ_i we can compute the planes $\mathbf{U}_i$ of the circles $\mathbf{c}_i$. The poles $\mathbf{Q}_i$ of $\mathbf{U}_i$ with respect to Σ are the vertices of cones Λ_i^* which touch Σ along the circles $\mathbf{c}_i$. If $\mathbf{c}_1$ is touched by a circle $\mathbf{c}$, the pole $\mathbf{Q}$ of the plane $\mathbf{U}$ of $\mathbf{c}$ must lie on Λ_1^*. Therefore the vertex $\mathbf{Q}$ of a cone which touches Σ along a filling circle $\mathbf{c}$, must lie on the intersection curve $\mathbf{l}$ of the cones Λ_1^*, Λ_2^*. Because of the common inscribed sphere of these two cones, their intersection curve is, in general, composed of two conics $\mathbf{l}_1$ and $\mathbf{l}_2$. Projecting the conics $\mathbf{l}_i$ from the origin yields two quadratic cones whose generators are the axes of possible intermediate cones Λ.

In case of Λ_1^* and Λ_2^* touching each other at a common generator the intersection curve consists of a conic $\mathbf{l}_1$ and the common generator $\mathbf{l}_2$. Points $\mathbf{Q}$ of $\mathbf{l}_2$ do not lead to useful solutions of intermediate cones Δ.

To compute the planes $\mathbf{V}_i$ of the conics $\mathbf{l}_i$, we first note that they must lie in the pencil spanned by $\mathbf{U}_1 = (u_{10} : u_{11} : u_{12} : u_{13})$ and $\mathbf{U}_2 = (u_{10} : u_{11} : u_{12} : u_{13})$, hence

$$\mathbf{V}_i = \mathbf{U}_1 + \lambda_i \mathbf{U}_2.$$

With Figure 2.2 one verifies that the cross ratio $\mathrm{cr}(\mathbf{U}_1, \mathbf{U}_2, \mathbf{V}_1, \mathbf{V}_2)$ equals -1 and that $\mathbf{V}_1, \mathbf{V}_2$ are conjugate with respect to Σ, i.e., the pole of $\mathbf{V}_1$ with respect to Σ lies in $\mathbf{V}_2$. This leads to

$$\lambda_{1,2} = \pm\sqrt{\frac{u_{11}^2 + u_{12}^2 + u_{13}^2 - u_{10}^2}{u_{21}^2 + u_{22}^2 + u_{23}^2 - u_{20}^2}}.$$

The orientation of the set of generators of the osculating cones Δ_i in the sense of increasing parameters leads to orientations of $\mathbf{c}_i$. Thus only one of the two conics $\mathbf{l}_i$, say $\mathbf{l}_1$, can lead to suitable solutions.

The computation of $\mathbf{l}_1$ and the resulting cones Λ and Δ may proceed as follows. We represent any segment of the circle $\mathbf{c}_1$ as a rational quadratic Bézier curve (see, for instance, Piegl and Tiller [34]). Its Bézier points shall have the correctly normalized homogeneous coordinates $\mathbf{B}_i^1,\ i = 0, 1, 2$. Then a homogeneous representation of the circle is given by

$$\mathbf{C}_1(t) = (1-t)^2\mathbf{B}_0^1 + 2t(1-t)\mathbf{B}_1^1 + t^2\mathbf{B}_2^1.$$

We use a projective parameter line P^1 described by homogeneous parameters t_0, t_1 with $t = t_1/t_0$ and parameterize the entire circle by

$$\mathbf{C}_1(t_0, t_1) = (t_0 - t_1)^2\mathbf{B}_0^1 + 2t_1(t_0 - t_1)\mathbf{B}_1^1 + t_1^2\mathbf{B}_2^1.$$

Projecting $\mathbf{C}_1$ from the center $\mathbf{Q}_1$ onto the plane $\mathbf{V}_1$ yields the conic $\mathbf{l}_1$. Using the projective invariance of the rational Bézier representation, we can represent $\mathbf{l}_1$ by applying the projection with matrix A_1 to the Bézier points $\mathbf{B}_i^1$. We get the Bézier points $\mathbf{B}_i^l = A_1 \cdot \mathbf{B}_i^1$ of $\mathbf{l}_1$. The projection from the plane $\mathbf{V}_1$ to $\mathbf{U}_2$ with center $\mathbf{Q}_2$ yields a Bézier representation of the circle $\mathbf{c}_2$ with Bézier points $\mathbf{B}_i^2$. To each $t = t_1 : t_0$, the points $\mathbf{C}_1(t), \mathbf{C}_2(t)$ determine the generators with vectors

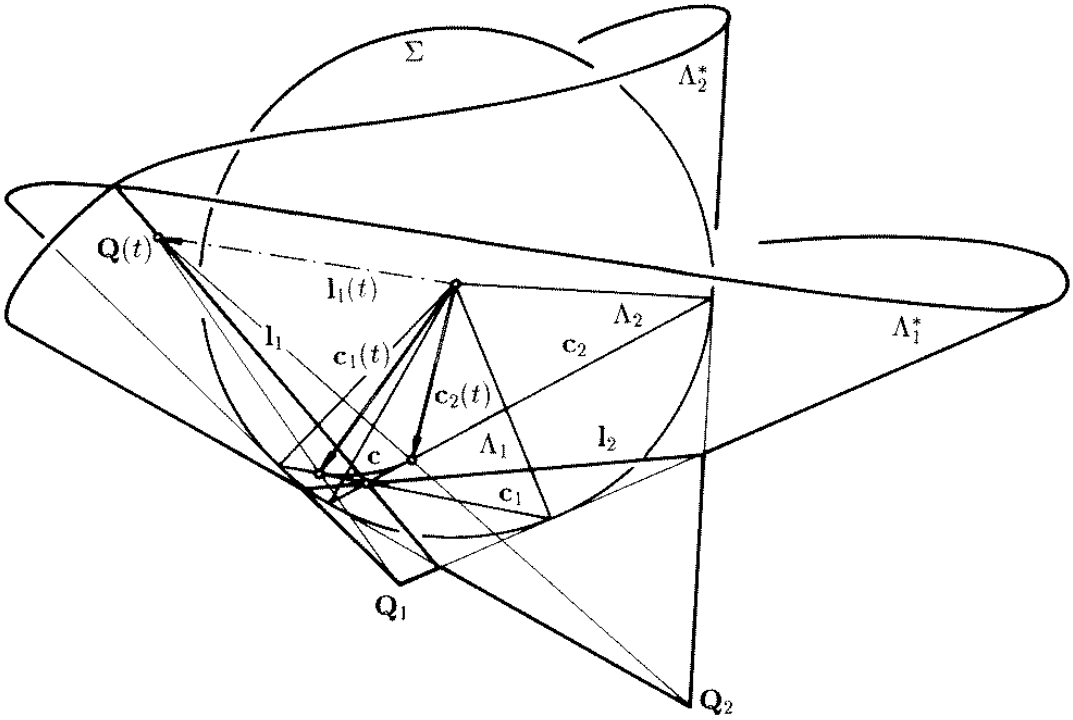

Figure 2.2: Construction of corresponding generators $\mathbf{c}_1(t)$, $\mathbf{c}_2(t)$

$\mathbf{c}_1(t), \mathbf{c}_2(t)$, along which a joining cone $\Lambda(t)$ with axis vector $\mathbf{l}_1(t)$ is touching the cones Λ_1, Λ_2. We summarize:

Theorem 2.1 *Given two oriented cones of revolution Λ_1, Λ_2 with common vertex, there is a one parameter set of cones of revolution Λ which smoothly join Λ_i while preserving the cones' orientation.*

If we translate the cones Λ_i back to their position Δ_i, not all $\Lambda(t)$ lead to solutions Δ of our problem. For a solution cone Δ, the generators $\mathbf{v}_i + u\mathbf{c}_i(t)$, $u \in \mathbb{R}$ of the cones Δ_i must intersect at the vertex $\mathbf{v}$ of Δ. Thus, only those t which satisfy the intersection condition

$$\det(\mathbf{c}_1(t), \mathbf{c}_2(t), \mathbf{v}_1 - \mathbf{v}_2) = 0 \tag{2.1}$$

belong to possible joining cones Δ. Equation (2.1) is a homogeneous quartic polynomial in t_0, t_1, which has up to four real solutions $t = t_1 : t_0$. Note that it is necessary to work with homogeneous parameters, since $t = 1 : 0$ may lead to a useful solution.

We will now look at the four possible solutions in detail. If $\mathbf{c}_1(t) = \mathbf{c}_2(t)$ is the vector of a common generator of Λ_1 and Λ_2 we get a solution for equation (2.1) which cannot be used to construct a joining cone Δ of Δ_i, though. As there are two common points of the two circles $\mathbf{c}_1, \mathbf{c}_2$, counted algebraically, there only remain two solutions for joining cones Δ which need not be real for arbitrary spatial position of cones Δ_i.

In our problem the cones Δ_i are osculating cones of a given developable surface Γ, however, touching Γ along generators e_i. By applying tools of Euclidean Laguerre geometry we will prove in section 3.3.2

Theorem 2.2 *Let Γ be a piecewise C^∞ developable surface. To any osculating cone $\Delta(t_1)$ of Γ to parameter t_1, there exists a parameter interval $U =]t_1, t_1 + \Delta t] \subset \mathbb{R}$ such that the osculating cones $\Delta(t_1)$ and $\Delta(t_2), t_2 \in U$ can be smoothly joined with a cone Δ. The joining cone Δ is real and joins Δ_1 and Δ_2 with G^1-continuity while preserving the orientation of Δ_i.*

To complete the discussion of the general case, we consider the case of Δ_i, say Δ_1, being an osculating cylinder. Let $\mathbf{c}_1$ determine the direction of its generators. The line $\lambda\mathbf{c}_1,\ \lambda \in \mathbb{R}$ can be interpreted as a degenerated cone Λ_1 which intersects Σ in the point $\mathbf{Q}_1$. Λ_1^* degenerates into the tangent plane of Σ at $\mathbf{Q}_1$. The intersection curve $\mathbf{l}_1 = \Lambda_1^* \cap \Lambda_2^*$ contains the points $\mathbf{Q}$ corresponding to filling circles $\mathbf{c}$. Again a projective mapping of corresponding generators of Δ_1 and Δ_2 is determined which leads to the solutions for Δ.

2.1.1 Special cases

In the previous section we have already treated the approximation of general cones with osculating cone spline surfaces. Unlike the general case there is a one parameter set of joining cones, see Theorem 2.1. Note that this contains the solution of finding a *spherical osculating arc spline* approximating a spherical curve: From the spherical curve one computes osculating circles c_i to parameters $t_1, \ldots, t_n$ and obtains a one parameter set of intermediate arcs to join successive osculating circles. In analogy to the planar case treated by Meek and Walton [28], one could show that appropriate choices within this solution set will yield a high accuracy approximation scheme.

Of course, this planar scheme is appropriate for the approximation of cylindrical surfaces as well as surfaces of constant slope (Fig. 1.11). In the last case all

osculating cones Δ_i have parallel axes and the same opening angle. Two consecutive cones Δ_1, Δ_2 in general intersect in a conic $\mathbf{l}_1$, which contains the possible vertices of connecting cone segments.

2.2 Examples

We apply the algorithm of osculating cone splines to the example in Figure 1.13. Using four generators e_i plus osculating cones Δ_i of our tangent surface as input data, we compute the three filling cone segments and get an approximation of Γ with seven cone segments (Fig. 2.3), one more than we got using four Hermite elements (e_i, τ_i). Note that the vertices $\mathbf{v}_i$ of the given cones Δ_i must lie on the line of regression but not the vertices of the intermediate cones. Using only two osculating cones Δ_1, Δ_2 of the same surface Γ results in a satisfying approximation quality even with few input data.

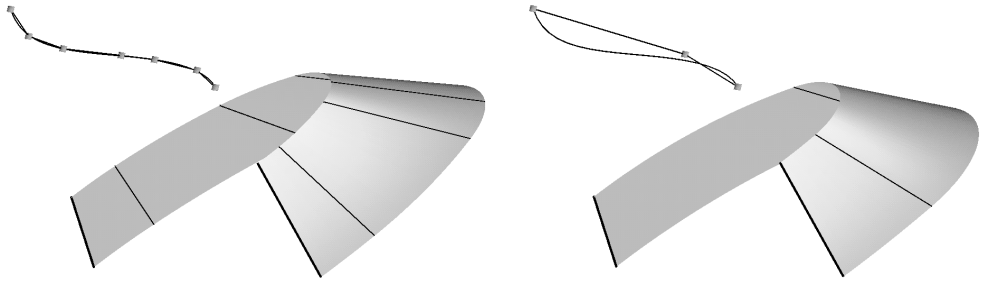

(a) (b)

Figure 2.3: Approximation of the developable surface of Fig. 1.13(a) with (a) 4, (b) 2 osculating cones as input data

2.3 Applications

2.3.1 Reconstruction of developable surfaces from scattered data

An important field of research is the reconstruction of surfaces from scattered data. Recently, some work has been done on the reconstruction of kinematic surfaces [8, 36, 38, 39]. These include helical surfaces with their subclass of rotational surfaces and moulding surfaces.

In [8] these methods have been applied to a disturbed point set of a developable surface which shall be approximated by a cone spline surface. The algorithms presented in this paper are robust against outliers. A basic step in this method is to find the best approximating cone of revolution to a point set. First the normal vectors are estimated and the axis is determined by least squares methods with non-linear constraints. All data points are rotated into a plane through this axis and the best fitting line to this data is chosen as generator.

Given the point cloud of a developable surface (Figure 2.4(a)) a region is iteratively determined which is well approximated by a single cone. A rough segmentation of the data points with the help of the Gaussian image supports the region growing algorithm. For an approximating cone of revolution two boundary planes through the axis are determined that enclose a wedge with only well-approximated data points. At the border of the initial region one chooses another seed point and repeats the procedure to get a set of cone segments Δ_i (Figure 2.4(b)) which are estimations of the osculating cones of the original surface. The cones Δ_i are not joined, however.

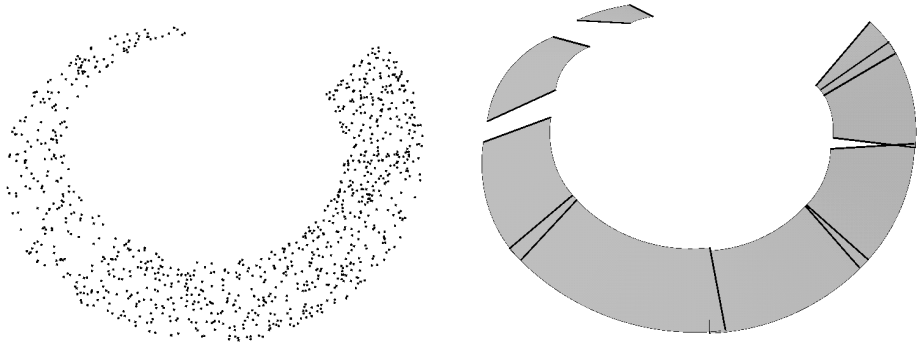

(a) (b)

Figure 2.4: (a) Point cloud, (b) approximating cone segments

With the method described in chapter 2 one can find an intermediate cone Δ to each two consecutive cones Δ_i, Δ_{i+1}, resulting in a cone spline surface (Figure 2.5). One has to be aware of the possibility of complex solutions for the joining cones Δ, however. This may occur if the estimation of the cones by least squares methods produces bad estimations for the osculating cones.

A more stable algorithm to determine a cone spline surface can be obtained by applying the cone pair algorithm described in chapter 1. From each estimated cone segment Δ_i one generator and its tangent plane is chosen. From the fist and last cones we will take the boundary generators and from each of the other cone segments we will choose the middle generator. Figure 2.6 shows the resulting cone spline surface if the vertex distance is minimized.

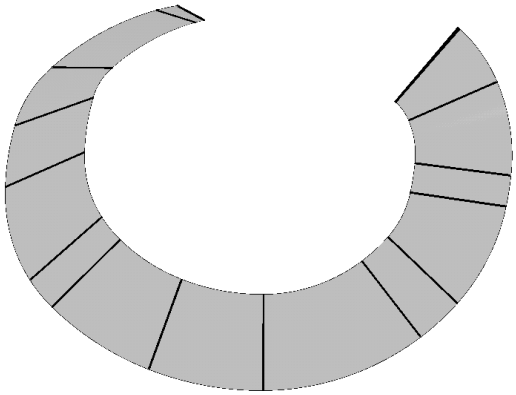

Figure 2.5: Approximating cone spline using cone segments of Fig. 2.4(b)

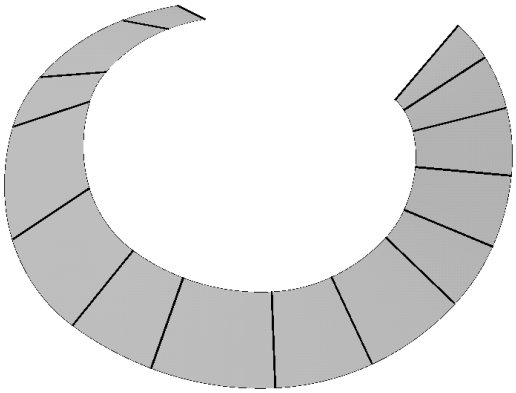

Figure 2.6: Approximating cone spline composed of cone pairs

2.3.2 Bending sequences and development

One major advantage of approximating a given developable surface by a cone spline surface is the simple development that does not need numerical integration. A cone segment Λ_0 is determined by the angle α_0 between generators and axis and the segment angle φ_0 (Fig. 2.7). Λ_0 can be bended into another cone segment Λ_1 with segment angle φ_1 and angle α_1 if

$$\varphi_1 \sin \alpha_1 = \varphi_0 \sin \alpha_0$$

is satisfied. The development of Λ_0 is a planar segment with segment angle

$$\varphi = \varphi_0 \sin \alpha_0.$$

Figure 2.8 shows a bending sequence (a) – (d) of a cone spline surface in which all segments are flattened out simultaneously. The distance between successive

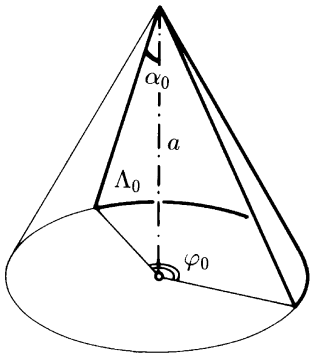

Figure 2.7: Cone segment

vertices remains constant during this process and a spatial arc spline as boundary curve is transferred into a planar arc spline of the development.

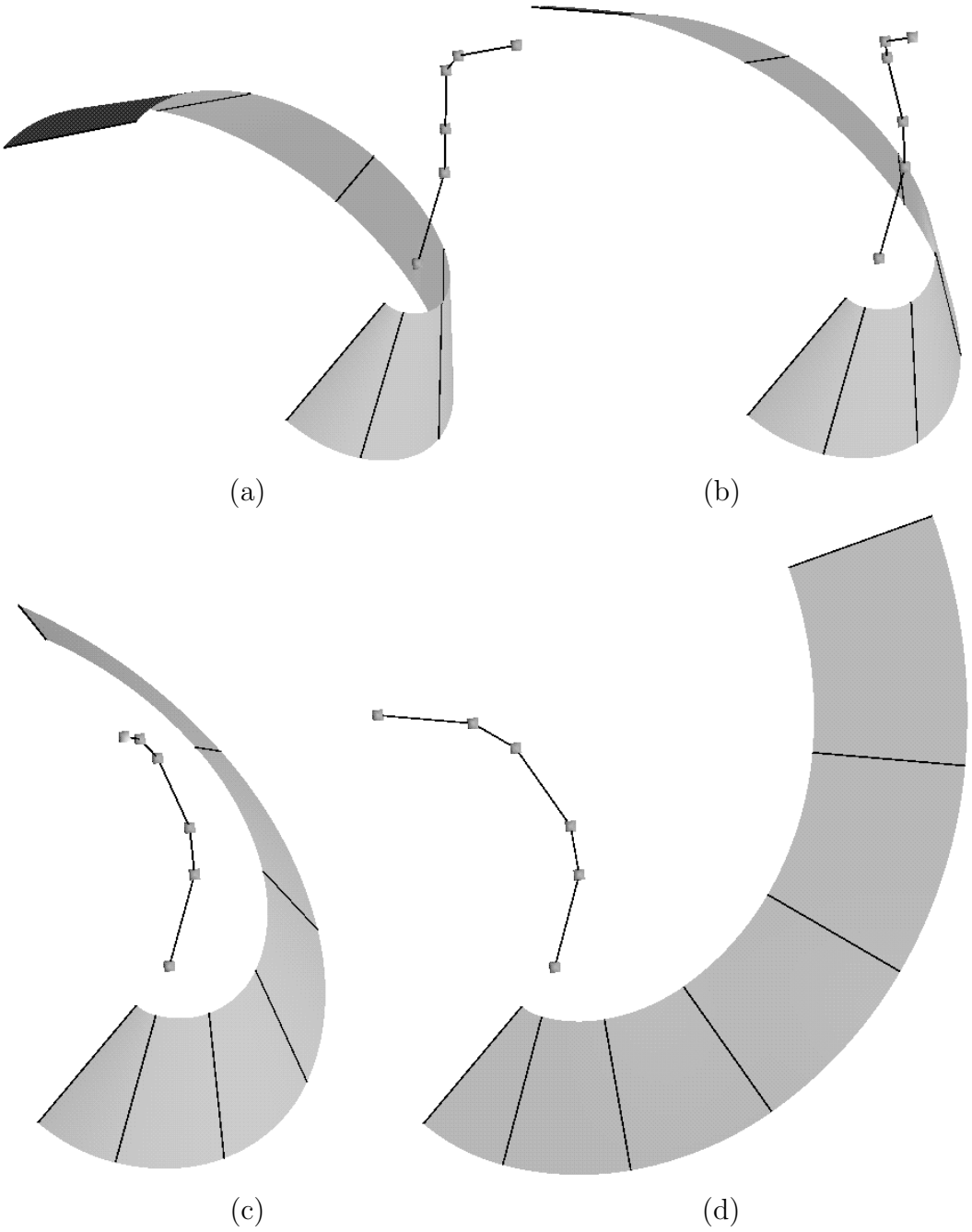

Figure 2.8: Bending sequence

Chapter 3

Spatial Isotropic Arc Splines

Developable surfaces are the envelopes of their one parameter set of tangent planes, i.e. they are dual to a spatial curve. For the aim of approximation of developable surfaces we are specially interested in cones of revolution which are special examples of developable surfaces whose tangent planes all touch a one parameter set of spheres.

This property motivates using 3-dimensional Euclidean Laguerre geometry in which the elements are *oriented spheres* and *oriented planes* of Euclidean 3-space.

We will first introduce different models of this geometry, all of them embedded in Euclidean 3- or 4-space E^3 or E^4. Especially useful for our purposes we will find the isotropic model presented in section 3.1.4 which provides a point representation of oriented planes, thus a curve representation of developable surfaces.

For the analytic treatment in E^3 we will either use the affine coordinate vector $\mathbf{x} = (x, y, z)$ to describe a point $\mathbf{x} \in E^3$ or its homogeneous coordinate vector $(x_0, x_1, x_2, x_3) = \lambda(1, x, y, z), \lambda \in \mathbb{R}\backslash\{0\}$ using the projective extension P^3 of E^3. In the following we will also use the notation $(x_0 : x_1 : x_2 : x_3)$ for homogeneous coordinates. Points at infinity are characterized by $x_0 = 0$. In E^4 we denote the affine coordinates of a point by $\mathbf{x} = (x, y, z, t)$ and its homogeneous coordinates in P^4 by $(x_0 : x_1 : x_2 : x_3 : x_4) = (1 : x : y : z : t)$.

3.1 3-dimensional Euclidean Laguerre space

3.1.1 The standard model

Let E^3 be real Euclidean 3-space, U the set of oriented planes $\mathbf{u}$ of E^3 and C the set of oriented spheres $\mathbf{c}$ including the points of E^3 as (non-oriented) spheres with radius zero. The elements of C are called *cycles*. The basic relation between oriented planes and cycles is that of *oriented contact*. An oriented sphere is said

to be in oriented contact with an oriented plane if they touch each other in a point and their normal vector in this common point is oriented in the same direction. The oriented contact of a point (nullcycle) and a plane is defined as incidence of point and plane.

Laguerre geometry is the survey of properties that are invariant under the group of so-called *Laguerre transformations* $\alpha = (\alpha_H, \alpha_C)$ which are defined by the two bijective maps

$$\alpha_H : H \to H, \alpha_C : C \to C \tag{3.1}$$

which preserve oriented contact and non-contact between cycles and oriented planes.

Analytically, a plane $\mathbf{u}$ is determined by the equation $u_0 + u_1 x + u_2 y + u_3 z = 0$ with normal vector (u_1, u_2, u_3). The coefficients u_i are homogeneous plane coordinates $(u_0 : u_1 : u_2 : u_3)$ of $\mathbf{u}$ in the projective extension P^3 of E^3. Each scalar multiple $(\lambda u_0 : \lambda u_1 : \lambda u_2), \lambda \in \mathbb{R}\backslash\{0\}$ describes the same plane, thus it is possible to use normalized homogeneous plane coordinates

$$\mathbf{u} = (u_0 : u_1 : u_2 : u_3), \text{with } u_1^2 + u_2^2 + u_3^2 = 1 \tag{3.2}$$

which are appropriate for describing *oriented* planes where the unit normal vector (u_1, u_2, u_3) determines the orientation of the plane.

An oriented sphere

$$\mathbf{c} = (x_m, y_m, z_m; r) \tag{3.3}$$

is determined by its midpoint $\mathbf{m} = (x_m, y_m, z_m)$ and signed radius r. Positive sign of r indicates that the normal vectors are pointing towards the outside of the sphere whereas in the case of negative sign of r they are pointing into the inside. Points of E^3 are cycles characterized by $r = 0$.

The relation of oriented contact is given by

$$u_0 + u_1 x_m + u_2 y_m + u_3 z_m + r = 0 \tag{3.4}$$

3.1.2 The cyclographic model

Let E^3 be embedded in Euclidean 4-space $E^4 = \{(x, y, z, t) \in \mathbb{R}^4\}$ as hyperplane $t = 0$. We will now map cycles and oriented hyperplanes of E^3 to points and special hyperplanes of E^4 in such a way that oriented contact is transformed to incidence.

A cycle $\mathbf{c} = (x_m, y_m, z_m; r) \in C$ is mapped to the point

$$\mathbf{C} = \zeta(\mathbf{c}) = (x_m, y_m, z_m, r) \in E^4. \tag{3.5}$$

The map $\zeta : C \to E^4$ is bijective and its inverse map ζ^{-1} is called *cyclographic map* or *isotropy projection* (see [6], for instance).

ζ determines the map ζ^* which maps an oriented plane $\mathbf{u} \in U; \mathbf{u} = (u_0 : u_1 : u_2 : u_3), u_1^2 + u_2^2 + u_3^2 = 1$ to the (non-oriented) hyperplane $\mathbf{U} = \zeta^*(\mathbf{u})$ of E^4 with homogeneous plane coordinates

$$\mathbf{U} = \zeta^*(\mathbf{u}) = (u_0 : u_1 : u_2 : u_3 : 1), \text{with } u_1^2 + u_2^2 + u_3^2 = 1. \tag{3.6}$$

The property of oriented contact of cycle $\mathbf{c}$ and oriented hyperplane $\mathbf{u}$ is equivalent to incidence of $\zeta(\mathbf{c})$ and $\zeta^*(\mathbf{u})$ which is given by equation (3.4). Note that each hyperplane $\zeta^*(\mathbf{u})$ encloses a Euclidean angle of $\gamma = \frac{\pi}{4}$ with the embedded hyperplane $E^3 : t = 0$ and will be called γ-hyperplane henceforth.

All oriented planes $\mathbf{u}$ being in oriented contact with a cycle $\mathbf{c}$ are mapped to γ-hyperplanes through $\mathbf{C}$ which envelope a quadratic hypercone $\Gamma(\mathbf{c})$ with vertex $\mathbf{C}$. The generators of $\Gamma(\mathbf{c})$ enclose an angle of γ with $t = 0$ and intersect the hyperplane $t = 0$ in the points of the sphere $\mathbf{c}$.

Let P^4 be the projective extension of E^4 and $\omega : x_0 = 0$ be the ideal plane. Each hypercone $\Gamma(\mathbf{c})$ intersects ω in the quadric

$$\Omega : x_0 = 0; x_1^2 + x_2^2 + x_3^2 - x_4^2 = 0, \tag{3.7}$$

where $(x_0 : \ldots : x_4)$ are homogeneous coordinates in P^4 and we see that all γ-hyperplanes are tangent to Ω. The polarity with respect to Ω determines a *pseudo-Euclidean orthogonality* $\perp_{pe}$ of lines g, $h \notin \omega$. If $\mathbf{g} = (g_1, g_2, g_3, g_4)$ and $\mathbf{h} = (h_1, h_2, h_3, h_4)$ denote the direction vectors of g and h this is written by

$$g \perp_{pe} h \Leftrightarrow \langle \mathbf{g}, \mathbf{h} \rangle_{pe} := g_1 h_1 + g_2 h_2 + g_3 h_3 - g_4 h_4 = 0, \tag{3.8}$$

which is equivalent to $(g \cap \omega)$ conjugate to $(h \cap \omega)$ with respect to Ω.

A line g which encloses an angle of γ, smaller than γ or greater than γ with the embedded E^3 is called *lightlike*, *spacelike* or *timelike*. A lightlike line g intersects ω in a point of Ω and is pe-orthogonal to itself. A spacelike line g intersects ω in the exterior of Γ and a timelike line g in the interior.

It is an important theorem of Euclidean Laguerre geometry that the equivalent of a Laguerre transformation α in the cyclographic model is a linear map of P^4 with $\omega \mapsto \omega$ and $\Omega \mapsto \Omega$. Therefore, a Laguerre transformation α is preserving pe-orthogonality and maps γ-hyperplanes onto γ-hyperplanes.

Let us now look at the representation of cones of revolution. In E^3 all oriented planes being in oriented contact with two different cycles $\mathbf{c}_1, \mathbf{c}_2$ generally envelope a cone of revolution. If the signed radii of $\mathbf{c}_1$ and $\mathbf{c}_2$ are equal this cone of revolution degenerates to a cylinder of revolution or (in case of two nullcycles $\mathbf{c}_1, \mathbf{c}_2$) to a pencil of planes.

The cyclographic image of the oriented tangent planes of a cone of revolution under ζ^* consists of the γ-hyperplanes through the line connecting $\mathbf{C}_1 = \zeta(\mathbf{c}_1)$ and $\mathbf{C}_2 = \zeta(\mathbf{c}_2)$. Only if the line $\mathbf{C}_1\mathbf{C}_2$ is spacelike there exist real γ-hyperplanes. If the line $\mathbf{C}_1\mathbf{C}_2$ is timelike there are no oriented hyperplanes in oriented contact with both cycles $\mathbf{c}_1$ and $\mathbf{c}_2$ which occurs in case of concentric cycles, for instance.

3.1.3 The Blaschke model

As we are more interested in the oriented tangent planes than in cycles it is appropriate to use a model of Euclidean Laguerre space in which oriented planes are represented by points. This can be achieved by applying a duality $\delta : (P^4)^* \to P^4$ to the cyclographic model described in the last section. The *Blaschke map* δ maps hyperplanes to points and is given by

$$\delta \circ \zeta^*(\mathbf{u}) = \delta(u_0 : u_1 : u_2 : u_3 : 1) = (1 : u_1 : u_2 : u_3 : u_0). \tag{3.9}$$

For all γ-hyperplanes $\zeta^*(\mathbf{u})$ there is $u_1^2 + u_2^2 + u_3^2 = 1$ so their δ images are points lying on the *Blaschke hypercylinder*

$$\Delta : x_1^2 + x_2^2 + x_3^2 = 1. \tag{3.10}$$

Using affine coordinates (x, y, z, t) one sees that the hypersurface Δ has a one dimensional generator line in t-direction through every point of the base surface $x^2 + y^2 + z^2 = 1$. Parallel and equally oriented planes possess the same normal vector (u_1, u_2, u_3) and therefore are mapped onto points lying on the same generator of Δ.

The Blaschke map δ further maps all hyperplanes through a given point $(x_0 : x_1 : x_2 : x_3 : x_4)$ to points lying in a hyperplane of P^4 with homogeneous plane coordinates $(x_4 : x_1 : x_2 : x_3 : x_0)$. A cycle $\mathbf{c}$ — viewed as envelope of its oriented tangent planes — is therefore mapped via $\delta \circ \zeta^*$ onto a hyperplanar intersection of Δ. The Laguerre transformations α appear as projective maps of P^4 with $\Delta \mapsto \Delta$.

The points of Δ together with its hyperplanar intersections and the automorphic linear maps of Δ build the so-called *Blaschke model* of Euclidean Laguerre geometry.

3.1.4 The isotropic model

Applying a stereographic projection σ to the Blaschke cylinder Δ one obtains the isotropic model of Euclidean Laguerre space. We will describe $\sigma : E^4 \to \bar{E}^3$ in affine coordinates. Let the projection center $\mathbf{z}$ have affine coordinates $\mathbf{z} = (0, 0, 1, 0)$ and the image hyperplane $\bar{E}^3$ be the hyperplane $z = 0$. We introduce an affine coordinate system $(\bar{x}, \bar{y}, \bar{z})$ in $\bar{E}^3$ so that the origins of E^4 and $\bar{E}^3$ coincide and

$$\bar{x} = x, \bar{y} = y, \bar{z} = t. \tag{3.11}$$

Let e be the generator line of Δ through $\mathbf{z}$ which is parallel to $\bar{E}^3$. The stereographic map $\sigma : \Delta \backslash e \to \bar{E}^3$ together with the cyclographic mapping ζ^* and the Blaschke map δ leads to

$$\Lambda := \sigma \circ \delta \circ \zeta^* : U \to \bar{E}^3, \tag{3.12}$$

which maps oriented hyperplanes $\mathbf{u} \in U$ of E^3 to points in $\bar{E}^3$. In coordinates this is written as

$$\Lambda(\mathbf{u}) = \sigma \circ \delta \circ \zeta^*(\mathbf{u}) = \frac{1}{1-u_3}(u_1, u_2, u_0). \tag{3.13}$$

Figure 3.1 illustrates the stereographic map σ for the one dimension lower case. The Figure can be interpreted as the restriction of $\sigma : \Delta \backslash e \to \bar{E}^3$ to the hyperplane $y = 0$.

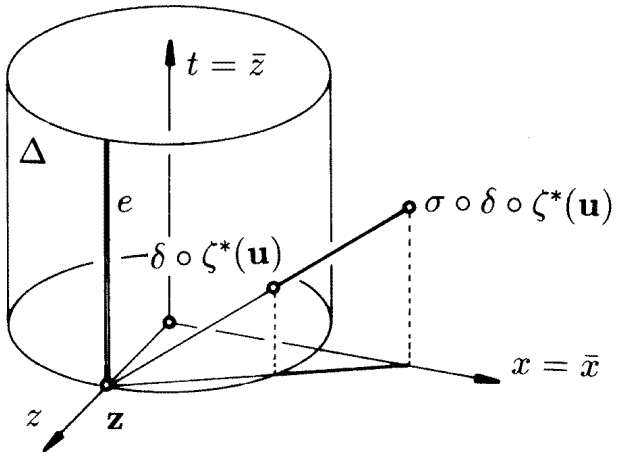

Figure 3.1: Stereographic map

The transition between the standard model and the isotropic model is described by Λ and its inverse Λ^{-1} which maps each point $\bar{\mathbf{x}} = (\bar{x}, \bar{y}, \bar{z})$ of $\bar{E}$ to an oriented plane in E^3 with normalized plane coordinates

$$\Lambda^{-1}(\bar{\mathbf{x}}) = \frac{1}{\bar{x}^2 + \bar{y}^2 + 1}(2\bar{z} : 2\bar{x} : 2\bar{y} : \bar{x}^2 + \bar{y}^2 - 1). \tag{3.14}$$

Formula (3.13) fails for oriented planes $\mathbf{u}$ with $u_3 = 1$, i.e. normal vector $(0, 0, 1)$. For such planes there is $\delta \circ \zeta^*(\mathbf{u}) \in e$ and σ maps all the points of e onto the point of infinity of the $\bar{z}$-axis. $\bar{E}^3$ together with this singular infinite point forms the *isotropic closure* I^3 of $\bar{E}^3$. The $\bar{z}$-direction is called *isotropic direction*.

Interpreting cycles $\mathbf{c}$ as their set of oriented tangent planes we obtain $\Lambda(\mathbf{c})$ as hyperplanar intersections of Δ. In the case that this hyperplane contains the projection center $\mathbf{z}$ the image $\Lambda(\mathbf{c})$ is a plane not parallel to the isotropic direction $\bar{z}$ otherwise $\Lambda(\mathbf{c})$ is a paraboloid of revolution with isotropic axis. In coordinates we have

$$\Sigma := \Lambda(\mathbf{c}) : 2\bar{z} + (\bar{x}^2 + \bar{y}^2)(r + z_m) + 2\bar{x}x_m + 2\bar{y}y_m + r - z_m = 0. \tag{3.15}$$

The surfaces Σ, defined by (3.15) are called *isotropic Möbius spheres*. The intersection of two isotropic Möbius spheres is either an ellipse whose top view (normal projection onto $\bar{z} = 0$) is a circle or a parabola with isotropic axis or a non-isotropic line. These curves are called *isotropic Möbius circles*. They are the the Λ-images of cones of revolution (including cylinders of revolution and pencils of planes).

In the isotropic model, Laguerre transformations are realized as special quadratic transformations, so-called *isotropic Möbius transformations*. These are bijective on the set of Möbius spheres Σ.

3.1.5 Differential geometry of curves in I^3

We will restrict our examinations to curves g: $\mathbf{g}(t) = (x(t), y(t), z(t))$ in I^3 which are regular and without inflection points and have no isotropic (z-parallel) tangents and isotropic osculating planes. Let $\widetilde{\mathbf{g}}(t) = (x(t), y(t))$ denote its normal projection into the xy-plane. To determine the isotropic osculating circle c of g at a point $\mathbf{g}(t_0)$ we intersect the cylinder of revolution through the osculating circle $\widetilde{c}$ of $\widetilde{g}$ at $\widetilde{\mathbf{g}}(t_0)$ with the osculating plane in $\mathbf{g}(t_0)$.

The semidefinite scalar product $\langle\rangle_i$ of two vectors $\mathbf{x}_1 = (x_1, y_1, z_1)$ and $\mathbf{x}_2 = (x_2, y_2, z_2)$ given by

$$\langle \mathbf{x}_1, \mathbf{x}_2 \rangle_i = x_1 x_2 + y_1 y_2 \tag{3.16}$$

defines the *isotropic distance* d_i of two points $\mathbf{g}_1$ and $\mathbf{g}_2$ by

$$d_i(\mathbf{g}_1, \mathbf{g}_2) := \sqrt{\langle \mathbf{g}_2 - \mathbf{g}_1, \mathbf{g}_2 - \mathbf{g}_1 \rangle_i} \tag{3.17}$$

which is the Euclidean distance of $\widetilde{\mathbf{g}}_1$ and $\widetilde{\mathbf{g}}_2$. Thus, the *isotropic arc length* of a regular curve $\mathbf{g}(t)$ is given by

$$u := \int \sqrt{\dot{x}^2 + \dot{y}^2} dt = \int \|\dot{\widetilde{\mathbf{g}}}\| dt. \tag{3.18}$$

Note that the isotropic distance is a metric property in I^3 (see e.g. [45]) and is not invariant under isotropic Möbius transformations.

3.2 Isotropic biarc approximation of curves

We will briefly analyze the approximation of curves in I^3 with isotropic biarcs. Let $\mathbf{a}_1$ and $\mathbf{a}_2$ be two points of a given curve g and $\mathbf{p}_1, \mathbf{p}_2$ their tangent vectors which are normalized by $\langle \mathbf{p}_i, \mathbf{p}_i \rangle_i = 1$. The Hermite elements $(\mathbf{a}_i, \mathbf{p}_i), i = 1, 2$ shall now be connected by a pair of isotropic arcs c_1 and c_2 joined with G^1 continuity.

Transforming this problem back from I^3 to the standard model of Euclidean Laguerre geometry with the map Λ^{-1} we obtain the approximation of a developable surface $\Lambda^{-1}(g)$ by a pair of cone segments $\Lambda^{-1}(c_1), \Lambda^{-1}(c_2)$. $(\mathbf{a}_i, \mathbf{p}_i)$ are the Λ images of the (oriented) Hermite elements (τ_i, e_i). Thus, approximation with isotropic biarcs is equivalent to the cone pair approximation we investigated in chapter 1.

Completely analogous to the situation with Euclidean biarcs we define a control polygon for the Bézier representation of the isotropic biarc. The control points will be named by $\mathbf{a}_1, \mathbf{b}_1, \mathbf{c}, \mathbf{b}_2, \mathbf{a}_2$ (see Figure 3.2).

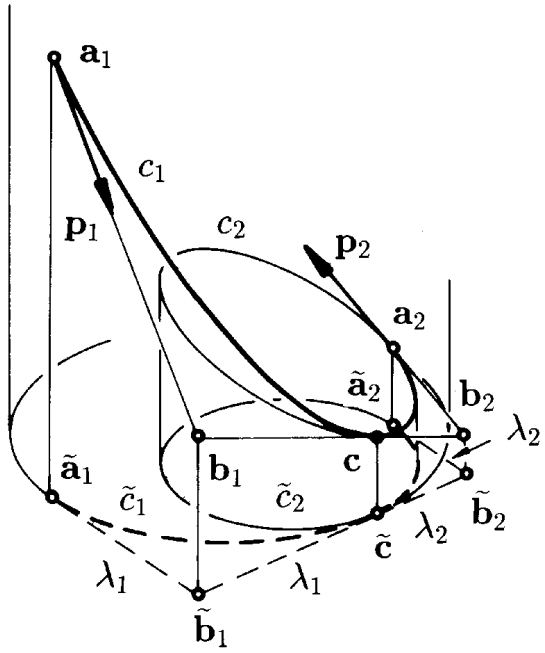

Figure 3.2: Isotropic biarcs

For $\mathbf{b}_1 = \mathbf{a}_1 + \lambda_1 \mathbf{p}_1$ and $\mathbf{b}_2 = \mathbf{a}_2 - \lambda_2 \mathbf{p}_2$ we obtain

$$\langle \mathbf{b}_2 - \mathbf{b}_1, \mathbf{b}_2 - \mathbf{b}_1 \rangle_i = (\lambda_1 + \lambda_2)^2,$$

as the normal projections $\tilde{c}_1, \tilde{c}_2$ of the isotropic arcs c_1, c_2 have to be Euclidean circles. Again there is a one parameter set of solutions which we can get by choosing $\mathbf{b}_1(\lambda_1)$ and computing $\mathbf{b}_2(\lambda_2)$. The junction point $\mathbf{c}$ can be computed by

$$\mathbf{c} = \frac{\lambda_2 \mathbf{b}_1 + \lambda_1 \mathbf{b}_2}{\lambda_1 + \lambda_2}.$$

For the Bézier representation of c_i we have weights 1 at $\mathbf{a}_i$ and $\mathbf{c}$ and weights w_i at $\mathbf{b}_i$ which satisfy

$$|w_i| = \frac{|\langle \mathbf{b}_i - \mathbf{a}_i, \mathbf{c} - \mathbf{a}_i \rangle_i|}{d_i(\mathbf{a}_i, \mathbf{b}_i) d_i(\mathbf{a}_i, \mathbf{c})}.$$

The sign of w_1 and w_2 have to be chosen equal to the sign of λ_1 and λ_2 (compare with the Euclidean case).

The following result on isotropic biarcs is an analogue to the results in [50] and [12] in Euclidean 3-space and can be derived from our investigations on approximation with cone pairs in chapter 1. After transferring these results into the isotropic model I^3 we obtain:

Theorem 3.1 *All the isotropic biarcs c_1, c_2 joining the Hermite elements $(\mathbf{a}_i, \mathbf{p}_i), i = 1, 2$ lie on an isotropic sphere Σ which is uniquely determined by $(\mathbf{a}_i, \mathbf{p}_i)$. The junction point $\mathbf{c}$ varies on an isotropic circle c which lies on Σ and passes through $\mathbf{a}_1$ and $\mathbf{a}_2$.*

3.3 Isotropic osculating arc splines

Let $\mathbf{a}_1$ and $\mathbf{a}_2$ be two points of a given curve g in I^3 which is regular and has no isotropic tangents. The oriented isotropic circles c_1 and c_2 osculating g in $\mathbf{a}_1$ and $\mathbf{a}_2$ lie in the planes σ_1 and σ_2. Our aim is to find an isotropic circle c joining c_1 and c_2 with G^1 continuity in the junction points $\mathbf{c}_1$ and $\mathbf{c}_2$ (see Figure 3.3). With

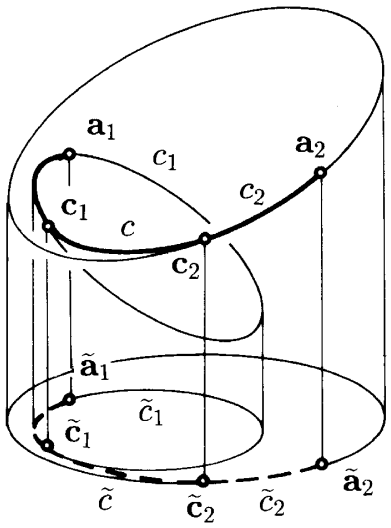

Figure 3.3: Isotropic osculating arcs

this method we are able to construct an isotropic arc spline approximating g so that every second arc is an isotropic osculating circle of g in a point $\mathbf{a}_i$. Although we use three arcs to join the two points $\mathbf{a}_1, \mathbf{a}_2$ the method produces an arc spline with about the same number of arcs as the biarc method does. This is because the next segment between $\mathbf{a}_2$ and $\mathbf{a}_3$ is continued with the isotropic arc c_2.

The survey of isotropic osculating arc splines is motivated by the fact that it is the Λ-image of the osculating cone spline approximation we dealt with in chapter 2: From a given developable surface $\Gamma = \Lambda^{-1}(g)$ we choose certain generators to oriented tangent planes $\tau_i = \Lambda^{-1}(\mathbf{a}_i)$ and join two consecutive oriented osculating cones $\Delta_i = \Lambda^{-1}(c_i)$ by a cone segment $\Delta = \Lambda^{-1}(c)$.

As curves are easier to handle than surfaces it is often preferable to work with isotropic circles in I^3 than with cones of revolution in E^3. Therefore, in section 3.3.1 we will first analyze geometrically how to find an isotropic arc c joining two isotropic circles c_1, c_2 which are osculating a curve g to parameter values t_1, t_2. It is obvious from our previous investigations that we will in general obtain two solutions for c which need not be real. In section 3.3.2 we will be able to prove, however, that there is a real and useful solution arc c if the difference between the parameter values t_i is sufficiently small. In our proof we will simplify the geometric situation by applying an appropriate isotropic Möbius transformation $\alpha : I^3 \to I^3$.

3.3.1 Method

The normal projection of c_1, c, c_2 into the xy-plane is an (Euclidean) arc spline $\widetilde{c}_1, \widetilde{c}, \widetilde{c}_2$ which we will examine first. Note that the pre-images $\mathbf{u} = \Lambda^{-1}(\mathbf{x})$ and $\widetilde{\mathbf{u}} = \Lambda^{-1}(\widetilde{\mathbf{x}})$ of a point $\mathbf{x} \in I^3$ and its top projection $\widetilde{\mathbf{x}}$ are parallel planes and $\widetilde{\mathbf{u}}$ contains the origin $\mathbf{o} \in E^3$. The top view of the isotropic triarc c_1, c, c_2 therefore is equivalent to a translation of the cones $\Lambda^{-1}(\mathbf{c}), \Lambda^{-1}(\mathbf{c}_i)$ so that they possess the common vertex $\mathbf{o}$.

It is well known that there is a one parameter set of circles c being in oriented contact with $\widetilde{c}_1, \widetilde{c}_2$ (see for instance [29]). Quite recently the approximation quality of planar osculating arc splines has been analyzed in [28].

We will define a control polygon for the arc spline and denote its points by $\widetilde{\mathbf{a}}_1, \ldots, \widetilde{\mathbf{a}}_2$ (see Figure 3.4). After choosing the first junction point $\widetilde{\mathbf{c}}_1(\lambda_1)$, where λ_1 is a homogeneous parameter on the oriented circle c_1, the second junction point $\widetilde{\mathbf{c}}_2(\lambda_2)$ is uniquely determined. $\widetilde{\mathbf{c}}_1(\lambda_1) \mapsto \widetilde{\mathbf{c}}_2(\lambda_2)$ is a projective mapping. It is an important property that the middle control point $\widetilde{\mathbf{d}}$ of $\widetilde{c}$ has to lie on the chordal line $\widetilde{d}$ of the two circles $\widetilde{c}_1, \widetilde{c}_2$ since $\widetilde{d}$ contains all points whose tangential distances to $\widetilde{c}_1$ and $\widetilde{c}_2$ are equal. The equation of $\widetilde{d}$ in affine coordinates is

$$\widetilde{d} : 2\mathbf{x}(\widetilde{\mathbf{m}}_2 - \widetilde{\mathbf{m}}_1) - (r_1^2 - r_2^2) + (\widetilde{\mathbf{m}}_1^2 + \widetilde{\mathbf{m}}_2^2) = 0 \tag{3.19}$$

where r_i denote the radii and $\widetilde{\mathbf{m}}_i$ the midpoints of $\widetilde{c}_i$. For the implementation of the projective map $\widetilde{\mathbf{c}}_1(\lambda_1) \mapsto \widetilde{\mathbf{c}}_2(\lambda_2)$ it is helpful to be aware of the fact that the connecting lines of matching points $\widetilde{\mathbf{c}}_1$ and $\widetilde{\mathbf{c}}_2$ always pass through a point $\mathbf{z}$. This property can be verified as follows: Let $\varkappa_1$ equal the homothety with center

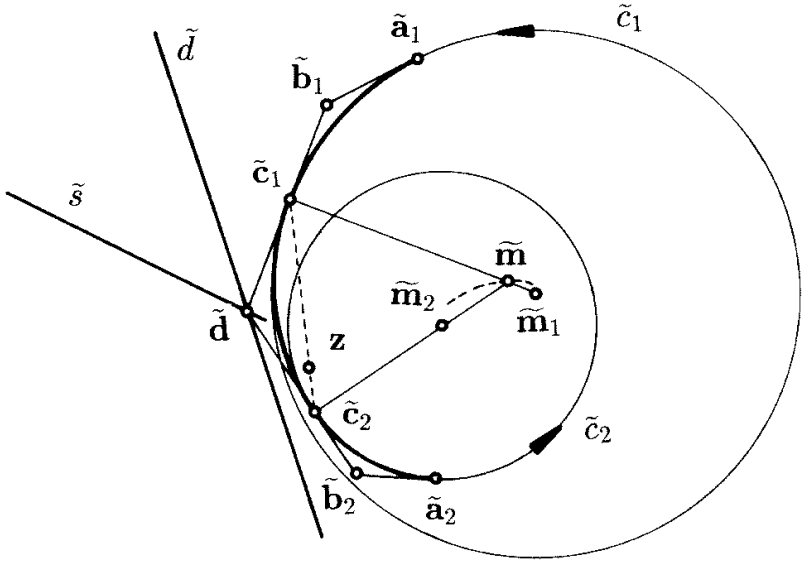

Figure 3.4: Planar Euclidean osculating arcs

$\mathbf{z}$ and $\varkappa_1(\tilde{c}_1) = \tilde{c}_2$, preserving the orientation of $\tilde{c}_i$. $\mathbf{z}$ is given by

$$\mathbf{z} = \frac{r_2}{r_2 - r_1}\widetilde{\mathbf{m}}_1 - \frac{r_1}{r_2 - r_1}\widetilde{\mathbf{m}}_2 \tag{3.20}$$

where the radii r_i of $\tilde{c}_i$ are oriented. Denote the $\tilde{c}_2$-automorphic harmonic perspectivity with center $\mathbf{z}$ by $\varkappa_2$. Then the composition $\varkappa = \varkappa_1\varkappa_2$ is a perspective collineation with center $\mathbf{z}$ and axis $\tilde{d}$ because the points of $\tilde{c}_1 \cap \tilde{c}_2$ are fixed under $\varkappa$. Now the restriction of $\varkappa$ to $\tilde{c}_1$ gives the projective map $\mathbf{c}_1(\lambda_1) \mapsto \mathbf{c}_2(\lambda_2)$.

Furthermore, the midpoints $\widetilde{\mathbf{m}}$ of the joining arcs lie on a conic with focal points $\widetilde{\mathbf{m}}_1$ and $\widetilde{\mathbf{m}}_2$ which directly follows from the basic definition of conics. Another way to realize the projective map $\tilde{\mathbf{c}}_1 \mapsto \tilde{\mathbf{c}}_2$ is to choose $\tilde{\mathbf{c}}_1$ and thus finding $\tilde{\mathbf{d}}$ by intersecting the tangent in $\tilde{\mathbf{c}}_1$ with $\tilde{d}$. Laying a tangent from $\tilde{\mathbf{d}}$ to $\tilde{c}_2$ one gets $\tilde{\mathbf{c}}_2$ which is unique because both circles $\tilde{c}_i$ are oriented.

We will now return to the spatial problem in I^3: a possible solution arc $\tilde{c}$ with junction points $\tilde{\mathbf{c}}_i$ of the planar problem does not necessarily lead to a solution arc c of the spatial problem because the tangents t_i in $\mathbf{c}_i$ to c_i generally lie in different osculating planes σ_1 and σ_2 and need not have a point $\mathbf{d}$ in common. As this point $\mathbf{d}$ cannot but lie on the intersection line $s = \sigma_1\sigma_2$ it is necessary for $\tilde{\mathbf{d}}$ to lie on both $\tilde{d}$ and the top projection $\tilde{s}$ of s. If $\tilde{\mathbf{d}}$ lies outside of $\tilde{c}_1$ and $\tilde{c}_2$ one gets two real solution arcs c. One just has to lay both tangents out of $\tilde{\mathbf{d}}$ to $\tilde{c}_i$ and thus determine the junction points while taking care of the circles' orientation.

In the special cases of $\sigma_1 = \sigma_2$ and $\tilde{s} = \tilde{d}$ there is a one parameter set of isotropic solution arcs c joining c_1 and c_2. This happens exactly if c_1 and c_2 lie on

a common isotropic Möbius sphere, i.e. a non-isotropic plane or a paraboloid of revolution. Reinterpreting with Λ^{-1}, we confirm the existence of a one parameter set of cones Δ in oriented contact with two given cones of revolution Δ_1, Δ_2 if both Δ_i are in oriented contact with a common sphere Σ. This includes the case of Δ_i possessing the same vertex $\mathbf{v}$ as the common vertex has to be interpreted as sphere with radius zero.

3.3.2 Feasibility of the solution

In order to show the reality and usefulness of a solution arc c we will prove

Theorem 3.2 *Let $\mathbf{g}(t)$ be a piecewise C^∞ curve in isotropic 3-space I^3. To any point $\mathbf{g}(t_1)$ there exists a parameter interval $U =]t_1, t_1 + \Delta t] \subset \mathbb{R}$ such that the points $\mathbf{g}(t_1)$ and $\mathbf{g}(t_2), t_2 \in U$ can be joined with an isotropic triarc in the following way: the first and the third arc of this triarc lie on the isotropic osculating circles c_1 and c_2 of $\mathbf{g}(t)$ to parameters t_1 and t_2 The joining isotropic arc c is real and joins c_1 and c_2 with G^1-continuity while preserving the orientation of c_i.*

Proof:

We apply an isotropic Möbius transformation $\alpha : I^3 \to I^3$ to the curve g such that the first isotropic osculating circle c_1 is mapped to the x-axis. As the order of contact between g and c_1 is not changed by α the x-axis is an inflection tangent to $\alpha(g)$.

Without loss of generality we can restrict ourselves to a curve $g = \mathbf{g}(t)$ which has an inflection point $\mathbf{g}(0)$ to parameter $t = 0$ at the origin $\mathbf{o}$. Let its inflection tangent be the x-axis and $\mathbf{g}(0) + \lambda_1 \dot{\mathbf{g}}(0) + \lambda_2 \mathbf{g}^{(3)}(0)$ be the xy-plane. A Taylor expansion of $\mathbf{g}(t)$ up to the fourth derivative is then given by

$$\mathbf{g}(t) = \begin{pmatrix} a_1 t + a_2 t^2 + a_3 t^3 + a_4 t^4 + O(t^5) \\ b_3 t^3 + b_4 t^4 + O(t^5) \\ c_4 t^4 + O(t^5) \end{pmatrix}, a_1, b_3, c_4 \in \mathbb{R}^+; a_i, b_i, c_i \in \mathbb{R} \quad (3.21)$$

with derivatives

$$\dot{\mathbf{g}}(t) = \begin{pmatrix} a_1 + 2a_2 t + 3a_3 t^2 + 4a_4 t^3 + O(t^4) \\ 3b_3 t^2 + 4b_4 t^3 + O(t^4) \\ 4c_4 t^3 + O(t^4) \end{pmatrix} \quad (3.22)$$

and

$$\ddot{\mathbf{g}}(t) = \begin{pmatrix} 2a_2 + 6a_3 t + 12a_4 t^2 + O(t^3) \\ 6b_3 t + 12b_4 t^2 + O(t^3) \\ 12c_4 t^2 + O(t^3) \end{pmatrix}. \quad (3.23)$$

We will compute the control points $\mathbf{c}_1, \mathbf{d}, \mathbf{c}_2$ of an isotropic arc c which is in oriented contact with the x-axis and the isotropic circle $c_2(t)$ which osculates g in $\mathbf{g}(t)$ (see Figure 3.5, where the connecting arc c has been omitted for reasons of clarity). The middle control point $\mathbf{d}$ is the intersection point of the osculating

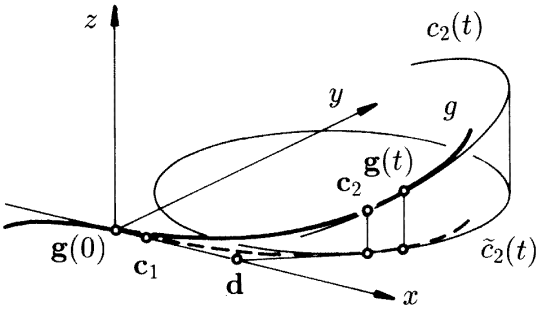

Figure 3.5: $\mathbf{g}(t)$ with inflection point $\mathbf{g}(0)$

plane σ_2 at $\mathbf{g}(t)$ with the x-axis. The junction point $\mathbf{c}_2$ can be computed by laying a tangent from $\mathbf{d}$ to $c_2(t)$. The last control point $\mathbf{c}_1$ on the x-axis is determined by

$$d_i(\mathbf{c}_1, \mathbf{d}) = d_i(\mathbf{c}_2, \mathbf{d}). \tag{3.24}$$

We will now calculate $\mathbf{c}_1, \mathbf{d}, \mathbf{c}_2$ in dependency on t and will show that for $t \to 0$, i.e. the touching point $\mathbf{g}(t)$ to $c_2(t)$ converges to $\mathbf{g}(0)$, we will obtain a useful arc c.

Defining the normal vector

$$\mathbf{n}(t) = \dot{\mathbf{g}}(t) \times \ddot{\mathbf{g}}(t) = \begin{pmatrix} 12c_4b_3t^4 + O(t^5) \\ -12a_1c_4t^2 + O(t^3) \\ 6a_1b_3t + 6(2a_1b_4 + a_2b_3)t^2 + O(t^3) \end{pmatrix} \tag{3.25}$$

of $\sigma_2(t)$, one gets

$$\sigma_2(t) : \mathbf{n}(t) \cdot \mathbf{x} = \mathbf{n}(t) \cdot \mathbf{g}(t)$$

and easily verifies

$$\mathbf{d}(t) = \sigma_2(t) \cap x\text{-axis} = \begin{pmatrix} \frac{1}{2}a_1t + O(t^2) \\ 0 \\ 0 \end{pmatrix}. \tag{3.26}$$

The following calculations will be made for the top projection $\widetilde{g}$ of g. The top view of $c_2(t)$ is the (Euclidean) osculating circle $\widetilde{c}_2(t)$ of $\widetilde{g}$ at $\widetilde{\mathbf{g}}(t)$. Its radius equals

$$\widetilde{r} = \frac{\|\dot{\widetilde{\mathbf{g}}}\|^3}{\det\left(\dot{\widetilde{\mathbf{g}}}, \ddot{\widetilde{\mathbf{g}}}\right)}.$$

Formulae (3.22) and (3.23) give

$$\tilde{r}^2(t) = \frac{1}{t^2}\left(\frac{a_1^4}{36b_3^2} + \frac{5a_1^3a_2b_3 - 2a_1^4b_4}{18b_3^2}t + O(t^2)\right). \tag{3.27}$$

The midpoint $\widetilde{\mathbf{m}}(t)$ of $\tilde{c}_2(t)$

$$\widetilde{\mathbf{m}}(t) = \tilde{\mathbf{g}}(t) + \frac{\|\dot{\tilde{\mathbf{g}}}(t)\|^2}{\det\left(\dot{\tilde{\mathbf{g}}}(t), \ddot{\tilde{\mathbf{g}}}(t)\right)} \cdot \dot{\tilde{\mathbf{g}}}^{\perp}(t)$$

simplifies to

$$\widetilde{\mathbf{m}}(t) = \begin{pmatrix} \frac{1}{2}a_1 t + O(t^2) \\ \frac{1}{t}\left(\frac{a_1^2}{6b_3} + \frac{5a_1a_2b_3 - 2a_1^2b_4}{6b_3^2}t + O(t^2)\right) \end{pmatrix}. \tag{3.28}$$

The square of the distance $\widetilde{R}(t)$ between $\mathbf{d}(t)$ and $\widetilde{\mathbf{m}}(t)$ equals

$$\widetilde{R}^2(t) = (\widetilde{\mathbf{m}}(t) - \mathbf{d}(t))^2 = \frac{1}{t^2}\left(\frac{a_1^4}{36b_3^2} + \frac{5a_1^3a_2b_3 - 2a_1^4b_4}{18b_3^2}t + O(t^2)\right). \tag{3.29}$$

Using coefficients of higher order in t, which have been omitted in formulae (3.27) and (3.29), one verifies for the power $\widetilde{p}(t)$ of the point $\mathbf{d}(t)$ with respect to the circle $\tilde{c}_2(t)$

$$\widetilde{p}(t) = \widetilde{R}^2(t) - \tilde{r}^2(t) = \frac{1}{12}a_1^2t^2 + O(t^3). \tag{3.30}$$

The value of $\widetilde{p}(t)$ is positive if t is sufficiently small. Thus, $\mathbf{d}(t)$ lies outside of $\tilde{c}_2(t)$ and $\tilde{\mathbf{c}}_2(t)$ and $\mathbf{c}_2(t)$ are real.

The power $\widetilde{p}(t)$ is the square of the distance of $\mathbf{d}(t)$ and $\tilde{\mathbf{c}}_2(t)$ and together with (3.24) we have

$$\widetilde{p}(t) = (\mathbf{d}(t) - \tilde{\mathbf{c}}_2(t))^2 = (\mathbf{d}(t) - \tilde{\mathbf{c}}_1(t))^2.$$

(3.26) and (3.21) show that the squares of the distances of $\mathbf{d}(t)$ to $\mathbf{o} = \tilde{\mathbf{g}}(0)$ and $\tilde{\mathbf{g}}(t)$ simplify to

$$(\mathbf{d}(t) - \tilde{\mathbf{g}}(0))^2 = (\mathbf{d}(t) - \tilde{\mathbf{g}}(t))^2 = \frac{1}{4}a_1^2t^2 + O(t^3) \tag{3.31}$$

which is greater than $\widetilde{p}(t)$ in formula (3.30). This shows that for small t the x-coordinate of $\mathbf{c}_1(t)$ is positive and the x-coordinate of $\mathbf{c}_2(t)$ is smaller than the x-coordinate of $\mathbf{g}(t)$ (see Figure 3.5). □

Chapter 4

Spatial Osculating Arc Splines

In the last section 3.3 we examined how to join two isotropic Möbius circles by an isotropic Möbius arc. This led to an isotropic osculating arc spline that approximated a given spatial curve in isotropic 3-space I^3.

It is natural to adapt the methods described above to Euclidean 3-space E^3. Let $g = \mathbf{g}(t)$ be a spatial curve in E^3 and $c_1, \ldots, c_n$ the osculating circles of g to parameters $t_1, \ldots, t_n$. Now each two consecutive osculating circles c_i, c_{i+1} shall be joined by an arc with G^1 continuity at the junction points. Thus, the given curve $g \in E^3$ is approximated by an arc spline where every second arc is an osculating arc of g. We will call such an arc spline *spatial osculating arc spline* henceforth.

Note that the case of g being a *planar* curve has been analyzed in [28]. Also, in section 3.3.1 the construction of planar osculating arc splines has been briefly discussed from a geometric point of view (see Fig. 3.4). The case of g being a *spherical* curve we have already treated in sections 2.1 and 2.1.1. Obviously results on spherical curve approximation can be derived from the planar case by stereographically projecting the plane onto a sphere. We know that in both cases there exists a one parameter set of solution arcs joining two given (oriented) circles. In the following we will restrict ourselves to the non-planar and non-spherical case.

In section 4.1 we will first present a geometric method of finding an arc c connecting two oriented circles in E^3. Note, that we will tacitly allow a circle to degenerate to a straight line which one can interpret as a circle with infinite radius. We will briefly consider all the special cases and see that there are two complex solutions in the general case.

It is natural to introduce 3-dimensional Euclidean Möbius geometry in section 4.2 since the set of Euclidean Möbius circles is comprised of straight lines and Euclidean circles. Similar to section 3.3.2 we will use a Möbius transformation in order to simplify the proof of Theorem 4.1 in section 4.3: two osculating circles

c_1, c_2 of a curve g can be joined by a real and useful arc c as long as the difference of parameters t_1, t_2 associated with c_1, c_2 is small enough.

In section 4.4 we will take a closer look at the approximation errors and propose an algorithm for a good segmentation of the given curve g. Choosing appropriate initial osculating circles c_i of g clearly has great influence on the quality of the approximation. Finally, in section 4.5 these results are applied to several examples.

4.1 Method

Let σ_1, σ_2 be the planes containing the oriented Euclidean circles c_1, c_2 in E^3. We first assume σ_i not to be parallel and treat special cases later. Our goal is to find control points $\mathbf{c}_1, \mathbf{d}, \mathbf{c}_2$ of an arc c joining c_1, c_2 while preserving the circles' orientation (Figure 4.1).

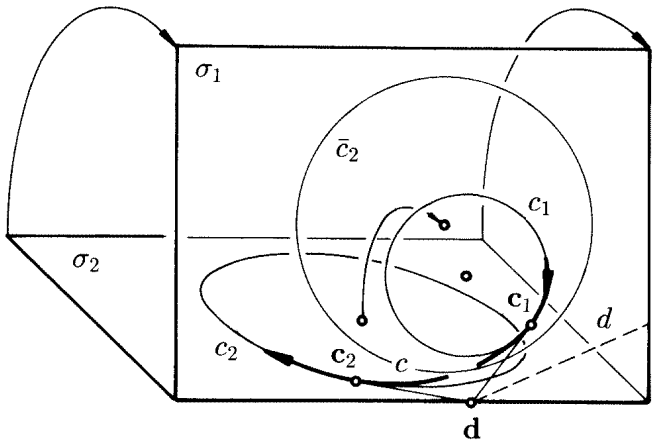

Figure 4.1: Spatial osculating arc spline

Obviously, the middle control point $\mathbf{d}$ has to lie on the line $s = \sigma_1 \cap \sigma_2$ and possess equal tangential distance to c_1 and c_2. To determine the location of $\mathbf{d}$ we will first rotate σ_2 around s such that σ_2 and σ_1 coincide. The chordal line d of c_1 and the rotated circle $\bar{c}_2$ in σ_1 contains all points of σ_1 with equal tangential distance to c_1 and $\bar{c}_2$. The only possible location of $\mathbf{d}$ is the intersection point of d with s. If $\mathbf{d}$ lies outside of c_1 and c_2 the missing two control points $\mathbf{c}_1$ and $\mathbf{c}_2$ of c can be found by laying tangents from $\mathbf{d}$ to c_1 and c_2. We obtain two solutions if the orientation of c_i is taken into consideration. These solutions are not real if $\mathbf{d}$ lies in the interior of c_1 and c_2. Note, that both possibilities to rotate σ_2 into σ_1 lead to the same point $\mathbf{d}$.

Special cases that have to be treated separately include the spherical case ($s = d$) and the planar case ($\sigma_1 = \sigma_2$), both of them leading to a one parameter set of solutions. If $\sigma_1 \parallel \sigma_2$, $\sigma_1 \neq \sigma_2$ the method given above does not work. Here, the junction points of a solution arc c lie in the common plane of symmetry of c_1 and c_2 (Figure 4.2).

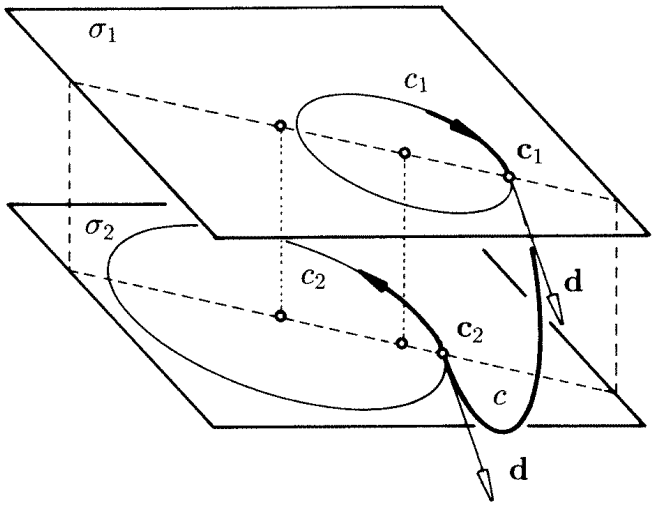

Figure 4.2: Special case: $\sigma_1 \parallel \sigma_2$

If one of the two circles, say c_1, is a line, the intersection of c_1 with σ_2 gives $\mathbf{d}$. Figure 4.3 shows one of the solution arcs which is real because $\mathbf{d}$ is lying on the outside of c_2. Last but not least, it is obvious that there are no connecting

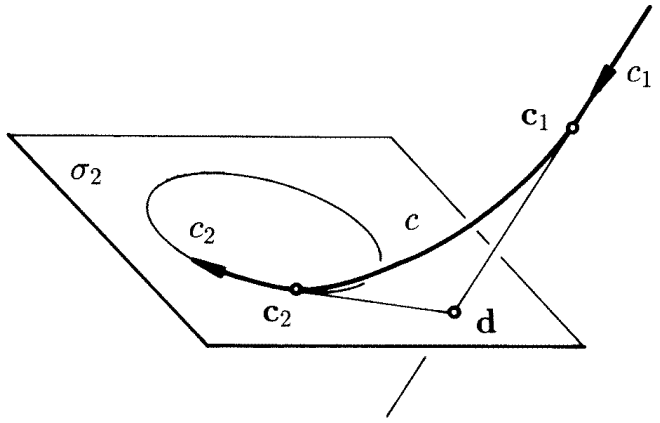

Figure 4.3: Special case: c_1 is a straight line

arcs in case of two skew lines c_1 and c_2. From a Möbius geometric point of view (compare with next section 4.2) this last case of skew lines is equivalent to two

oriented circles c_1, c_2 that intersect in a single point without touching each other in this point.

4.2 3-dimensional Euclidean Möbius geometry

Let E^3 be real Euclidean 3-space, P its point set and M the set of spheres and planes of E^3. We obtain the so-called *Euclidean conformal closure* ${E_M}^3$ of E^3 by extending the point set P by an arbitrary element $\mathbf{u} \notin P$ to $P_M = P \cup \{\mathbf{u}\}$. As an extension of the incidence relation we define that $\mathbf{u}$ lies in all planes but in none of the spheres. The elements of M are called *Euclidean Möbius spheres* and the intersection of two Möbius spheres is a so-called *Euclidean Möbius circle*. Euclidean Möbius geometry is the study of properties that are invariant under *Euclidean Möbius transformations*. A Möbius transformation is an incidence preserving composition of a bijective map of P_M and a bijective map of M.

Another model of this geometry we obtain by embedding E^3 in Euclidean 4-space E^4 as plane $t = 0$. Let $\sigma : \Sigma \backslash \{\mathbf{z}\} \to E^3$ be the stereographic projection of the unit hypersphere

$$\Sigma : x^2 + y^2 + z^2 + t^2 = 1 \tag{4.1}$$

onto E^3 with center $\mathbf{z} = (0, 0, 0, 1)$. Extending σ to $\bar{\sigma}$ with $\bar{\sigma} : \mathbf{z} \mapsto \mathbf{u}$ gives a new model of Euclidean Möbius geometry. The point set is that of $\Sigma \subset E^4$ and the Möbius spheres are the hyperplanar intersections of Σ since σ is preserving spheres. It is a central theorem of Euclidean Möbius geometry that all Euclidean Möbius transformations of this model are induced by an automorphic linear map $P^4 \to P^4$ of Σ, where P^4 denotes the projective extension of E^4.

4.3 Feasibility of the solution

Completely analogous to the isotropic case in 3.3.2 we state

Theorem 4.1 *Let $\mathbf{g}(t)$ be a piecewise C^∞ curve in Euclidean 3-space E^3. To any point $\mathbf{g}(t_1)$ there exists a parameter interval $U =]t_1, t_1 + \Delta t] \subset \mathbb{R}$ such that the points $\mathbf{g}(t_1)$ and $\mathbf{g}(t_2), t_2 \in U$ can be joined with a Euclidean triarc in the following way: the first and the third arc of this triarc lie on the Euclidean osculating circles c_1 and c_2 of $\mathbf{g}(t)$ to parameters t_1 and t_2. The joining Euclidean arc c is real and joins c_1 and c_2 with G^1-continuity while preserving the orientation of c_i.*

Proof: We apply a Euclidean Möbius transformation to the curve g such that the first osculating circle c_1 is mapped to the x-axis. Thus, we can restrict our calculations to curves $g = \mathbf{g}(t)$ with an inflection point at $\mathbf{g}(0) = \mathbf{o}$.

We will compute the control points $\mathbf{c}_1, \mathbf{d}, \mathbf{c}_2$ of an arc c which is in oriented contact with the x-axis and the osculating circle c_2 of g to parameter t. The middle control point $\mathbf{d}$ can be found as intersection point of the osculating plane σ_2 with the x-axis (Figure 4.4). The junction point $\mathbf{c}_2$ can be determined by

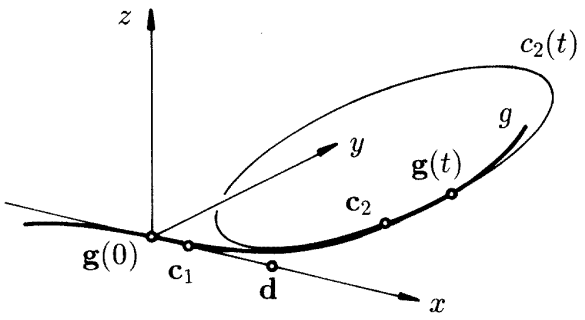

Figure 4.4: $\mathbf{g}(t)$ with inflection point $\mathbf{g}(0)$

laying a tangent from $\mathbf{d}$ to c_2 and $\mathbf{c}_1$ follows from

$$\|\mathbf{c}_1 - \mathbf{d}\| = \|\mathbf{c}_2 - \mathbf{d}\|. \tag{4.2}$$

The only difference to section 3.3.2 is that c_2 is a Euclidean circle and the distances in (4.2) are Euclidean ones.

We can use (3.21) to (3.23), (3.25) and (3.26) for the Taylor expansions of $\mathbf{g}(t), \dot{\mathbf{g}}(t), \ddot{\mathbf{g}}(t), \mathbf{n}(t)$ and $\mathbf{d}(t)$. The radius $r(t)$ of the (Euclidean) osculating circle $c_2(t)$ of g at $\mathbf{g}(t)$ equals

$$r = \frac{\|\dot{\mathbf{g}}\|^3}{\|\mathbf{n}(t)\|}$$

and with (3.22) and (3.25) simplifies to

$$r^2(t) = \frac{1}{t^2}\left(\frac{a_1^4}{36b_3^2} + \frac{5a_1^3a_2b_3 - 2a_1^4b_4}{18b_3^2}t + O(t^2)\right). \tag{4.3}$$

The midpoint $\mathbf{m}(t)$ of $c_2(t)$

$$\mathbf{m}(t) = \mathbf{g}(t) + \frac{\|\dot{\mathbf{g}}(t)\|^2}{\|\mathbf{n}(t)\|^2} \cdot (\mathbf{n}(t) \times \dot{\mathbf{g}}(t))$$

possesses Taylor expansions

$$\mathbf{m}(t) = \begin{pmatrix} \frac{1}{2}a_1 t + O(t^2) \\ \frac{1}{t}\left(\frac{a_1^2}{6b_3} + \frac{5a_1a_2b_3 - 2a_1^2b_4}{6b_3^2}t + O(t^2)\right) \\ \frac{a_1^2c_4}{3b_3^2} + O(t) \end{pmatrix}. \tag{4.4}$$

The square of the distance $R(t)$ between $\mathbf{d}(t)$ and $\mathbf{m}(t)$ equals

$$R^2(t) = (\mathbf{m}(t) - \mathbf{d}(t))^2 = \frac{1}{t^2}\left(\frac{a_1^4}{36b_3^2} + \frac{5a_1^3a_2b_3 - 2a_1^4b_4}{18b_3^2}t + O(t^2)\right) \tag{4.5}$$

which leads to

$$p(t) = R^2(t) - r^2(t) = \frac{1}{12}a_1^2t^2 + O(t^3)$$

for the power of $\mathbf{d}(t)$ with respect to c_2. If t is small enough the value of $p(t)$ is positive but smaller than

$$(\mathbf{d}(t) - \mathbf{g}(0))^2 = (\mathbf{d}(t) - \mathbf{g}(t))^2 = \frac{1}{4}a_1^2t^2 + O(t^3).$$

Therefore, a real and useful solution arc c exists which provides a triarc connection of $\mathbf{g}(0)$ and $\mathbf{g}(t)$. □

4.4 Segmentation

4.4.1 Error estimates

The approximation errors of a spatial arc spline can be judged easily. Let $\mathbf{x}$ be a point of the given curve $\mathbf{g}(t)$ and c one of the arc splines' segments with Bézier points $\mathbf{b}_i$ and midpoint $\mathbf{m}$ (Figure 4.5). It is computationally easy to check if the

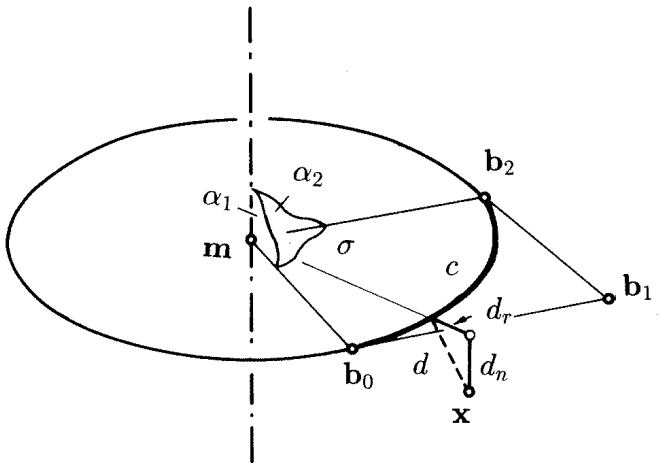

Figure 4.5: Distance of a point $\mathbf{x}$ to an arc c

point $\mathbf{x}$ lies in the wedge between the planes α_1 and α_2 through the rotation axis of c. The Euclidean distance of $\mathbf{x}$ to the circle segment c then is

$$d(\mathbf{x}, c) = \sqrt{d_n^2 + d_r^2}. \tag{4.6}$$

where d_n denotes the component lying normal to the circles' plane σ and d_r is the radial distance. In the following we will orient d_r such that $d_r > 0$ indicates that the normal projection of $\mathbf{x}$ onto σ lies outside of c. Also the orientation of c determines an orientation of σ and thus an orientation of d_n. In the degenerating case of c being a straight line segment the distance $d(\mathbf{x}, c)$ again is well-defined but we will not distinguish between radial and normal components.

If we choose a segmentation $\mathbf{g}(t_1), \ldots, \mathbf{g}(t_n)$ of the given curve $\mathbf{g}(t)$ the osculating circles to the parameters $t_1, \ldots, t_n$ will be used in the approximating arc spline. It is natural to select those points where the osculating circle approximates $\mathbf{g}(t)$ well. Let

$$\mathbf{g}(u) = \begin{pmatrix} u & - & \varkappa^2 \frac{u^3}{3!} & + & O(u^4) \\ & \varkappa \frac{u^2}{2!} & + & \varkappa' \frac{u^3}{3!} & + & O(u^4) \\ & & & \varkappa\tau \frac{u^3}{3!} & + & O(u^4) \end{pmatrix} \tag{4.7}$$

be the Taylor expansion of $\mathbf{g}(t)$ at the point $\mathbf{g}(0)$ with respect to arc length u (compare with (1.20)). The Frenet frame in $\mathbf{g}(0)$ is used as coordinate system and $\varkappa = \varkappa(0)$, $\varkappa' = \frac{d\varkappa}{du}(0)$ and $\tau = \tau(0)$ denote the differential invariants evaluated at $\mathbf{g}(0)$. The osculating arc c_0 at $\mathbf{g}(0)$ has midpoint

$$\mathbf{m}_0 = (0, \frac{1}{\varkappa}, 0)^T. \tag{4.8}$$

The third coordinate in (4.7) gives the normal component

$$d_n(u) = \frac{1}{6}\varkappa\tau u^3 + O(u^4) \tag{4.9}$$

of the distance $d(u)$ between $\mathbf{g}(u)$ and c_0. The radial component is

$$d_r(u) = \|\tilde{\mathbf{g}}(u) - \mathbf{m}_0\| - r_0$$

where $\tilde{\mathbf{g}}(u)$ is the normal projection of $\mathbf{g}(u)$ into the xy-plane and r_0 the radius of c_0. With (4.7), (4.8) and $r_0 = \frac{1}{\varkappa}$ its Taylor expansion simplifies to

$$d_r(u) = -\frac{1}{6}\varkappa' u^3 + O(u^4) \tag{4.10}$$

and together with (4.6) and (4.9) we have

$$d(u) = \frac{1}{6}\sqrt{\tau^2\varkappa^2 + \varkappa'^2}\, u^3 + O(u^4). \tag{4.11}$$

for the distance between $\mathbf{g}(u)$ and c_0.

The leading term of (4.11) provides us with a function

$$F(t) = \frac{1}{6}\sqrt{\tau(t)^2\varkappa(t)^2 + \varkappa'(t)^2} \tag{4.12}$$

such that $F(t_i)$ indicates the approximation quality of the osculating circle $c(t_i)$ for $t \to t_i$. $F(t_i) = 0$ is equivalent to $\varkappa'(t_i) = 0, \tau(t_i) = 0$ or $\varkappa'(t_i) = 0, \varkappa(t_i) = 0$. In the second case $c(t_i)$ degenerates to a straight line, in both cases $c(t_i)$ and $g = \mathbf{g}(t)$ hyperosculate, i.e. they are in contact of order 3.

4.4.2 Segmentation algorithm

A segmentation $t_0 = t_a, t_1, \ldots, t_n$ of the curve $\mathbf{g}(t), t \in [t_a, t_b]$ is practicable if the following three criteria hold true for each segment:

Criterion 1: The connecting circle of $c(t_i)$ and $c(t_{i+1})$ is real.

Criterion 2: The maximal error between the curve $\mathbf{g}(t), t \in [t_i, t_{i+1}]$ and the resulting triarc does not exceed a chosen error tolerance.

Criterion 3: Both of the two inner joining points of the triarc lie on the right side of the oriented osculating circles $c(t_i)$ and $c(t_{i+1})$ (compare with the bad case in Figure 4.6). Note, that in some cases a useful arc spline can be constructed, although criterion 3 is not fulfilled (see example 2, for instance). This depends on the joining point of the next arc segment, though.

Figure 4.6: Violation of Criterion 3

Possible segmentation algorithms include

- **The bisection method:** One chooses an evenly distributed segmentation with respect to arc length first. Each segment is bisected for which one of the criteria given above does not hold true. Clearly, this method is easy to implement but will not produce evenly distributed segmentations, in general.
- **Longest triarc method:** Let $t_0 = t_a$ be the first segmentation point. The next one, t_1, will be chosen as largest parameter value such that criteria 1 to 3 are still fulfilled. This procedure is repeated for the next segments. Thus, one minimizes the number of arc segments involved but completely ignores the geometric properties of the given curve. The approximation of a closed curve would give different results depending on the starting point, for instance.

Here a different approach will be proposed. An initial segmentation will be performed at the local minimas of the function $F(t)$ of 4.12. Figure 4.7 shows

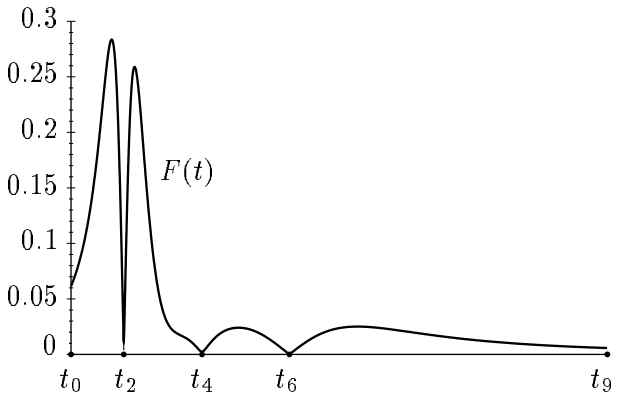

Figure 4.7: Function $F(t)$ for a polynomial curve of degree 4.

$F(t)$ for a polynomial curve of degree 4 which is taken from example 2 of section 4.5. The osculating arcs to parameters t_0, t_2, t_4, t_6, t_9 well approximate the curve $\mathbf{g}(t)$. These five segmentation points give four triarc segments. As each of the osculating circles $c(t_2), c(t_4), c(t_6)$ is used in two triarc segments the computed arc spline is composed of nine arc segments (see Figure 4.13). Figure 4.8 shows the approximation error of this initial approximation. Note, that in the third

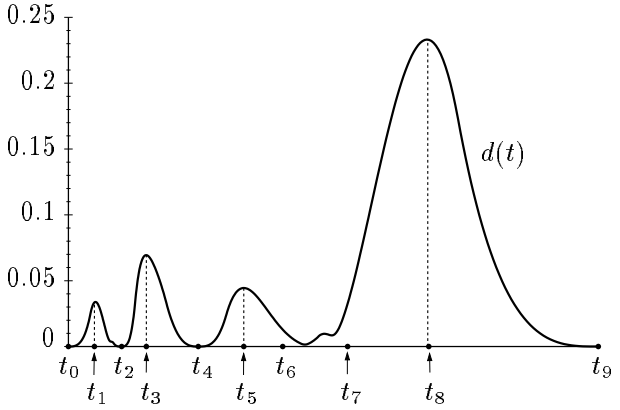

Figure 4.8: Approximation error $d(t)$ after initial segmentation

triarc segment $[t_4, t_6]$ criterion 3 is violated. The resulting arc spline still is useful although the segment on the osculating arc $c(t_6)$ is very short. In order to avoid such situations and in order to reduce the error to the desired accuracy one has to subdivide segments.

For the subdivision point we choose the peak value of the error function $d(t)$ within a segment (t_1, t_3, t_5, t_7). If $d(t)$ has two peaks of approximately the same

value (see for instance Fig. 4.10 (a), (b) or Fig. 4.15) one either splits in between or divides into three segments.

After computing the triarc of the segment $[t_6, t_8]$ still the error tolerance of 0.01 is exceeded at this segment (the corresponding figure for $d(t)$ is not given). Subdivision at the maximum error gives t_7. The final arc spline is presented in Figure 4.14 of the next section.

4.5 Examples

Example 1 Helical curve

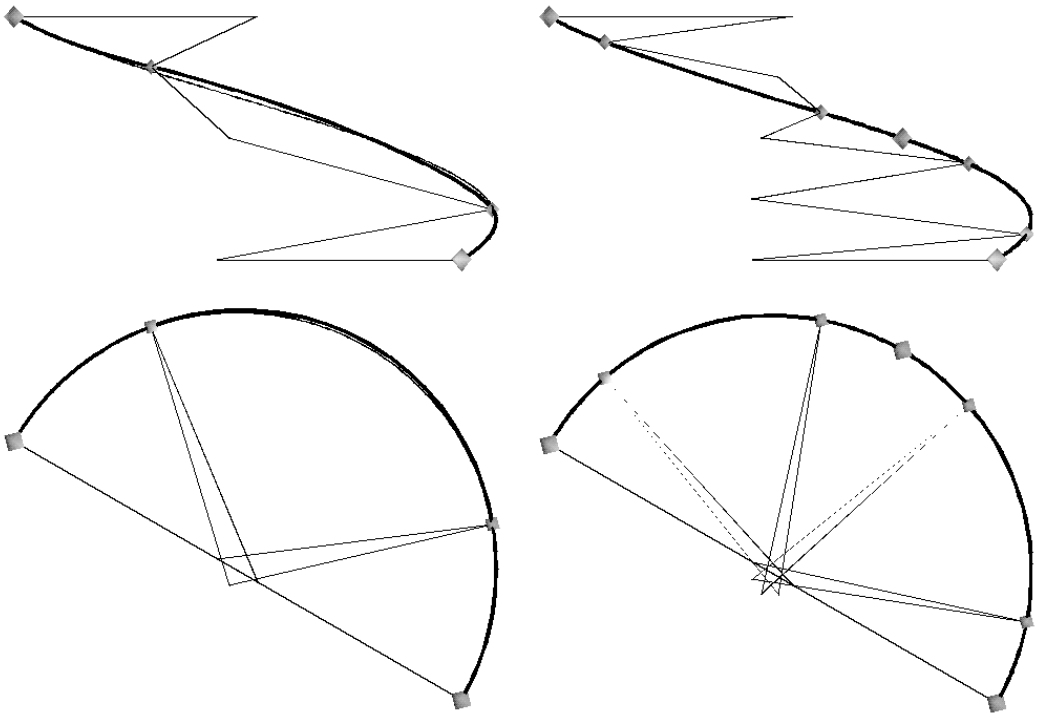

(a) (b)

Figure 4.9: Approximation with (a) one, (b) two triarc segments

Figure 4.9 (a) shows the approximation of a helical curve (thin curve) by one triarc segment (thick curve) in top view and front view. Figure 4.9 (b) shows the approximation of the same curve with two triarc segments. The big octahedrons indicate the curve points whose osculating circles were computed. The smaller octahedron are the joining points of different arc segments. In order to better

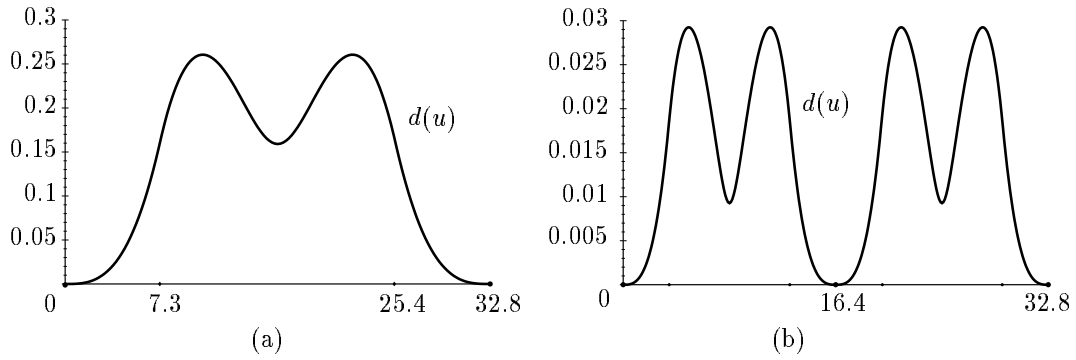

Figure 4.10: Approximation error $d(u)$ for (a) one, (b) two triarc segments

illustrate the spatial position of the arc segments their end points are connected to their midpoint with thin lines.

Figure 4.10 (a) and (b) contain diagrams showing the approximation error $d(u)$ of the helical curve to the arc splines. Here u is the arc length of the helix. The occurring error has its peaks at the middle arc segment which can also be clearly seen in Figure 4.9 (a). Note the different scalings in the diagrams Fig. 4.10 (a) and (b) which tend to disguise the fact that the error has decreased approximately by factor 1/8 because the segment has been bisected.

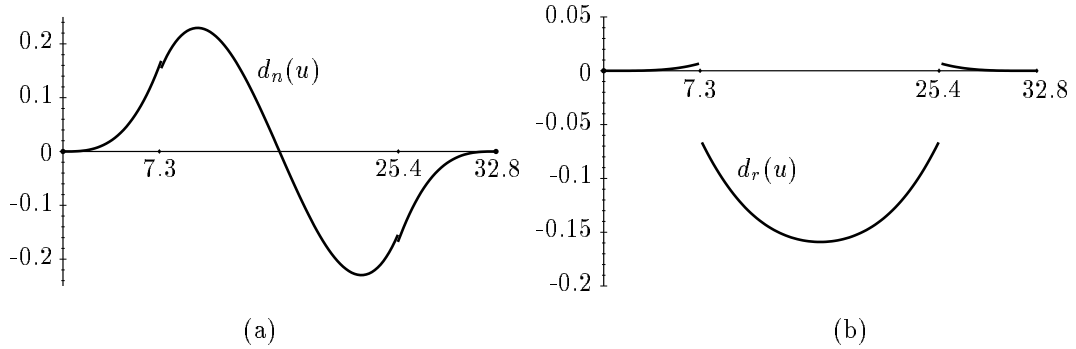

Figure 4.11: (a) Normal component $d_n(u)$, (b) radial component $d_r(u)$ of the approximation error $d(u)$ of Fig. 4.10(a)

In Figure 4.11 the error $d(u)$ of Fig. 4.10(a) is split into its normal and radial components $d_n(u)$ and $d_r(u)$. The function $d_n(u)$ shows that the helical curve lies on both sides of the plane of the middle arc segment. At the point of vanishing d_n the radial distance d_r reaches is maximum. While $d(u)$ is smooth the functions $d_n(u)$ and $d_r(u)$ have discontinuities at the junction points. This occurs because of the twist angle between the planes containing the adjacent arc segments. In the present example the angle between two consecutive planes equals 25.8°.

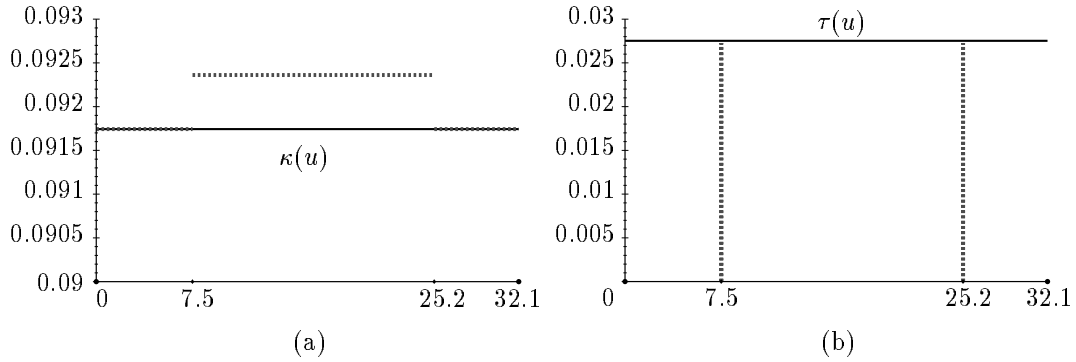

Figure 4.12: (a) Curvature and (b) torsion diagrams of a helical curve and its approximation with one triarc

Finally, in Figure 4.12 we look at curvature and torsion diagrams $\varkappa(u)$, $\tau(u)$ of the helical curve, both of them being constant functions. The dotted lines indicate the curvature and torsion profile of the approximating arc spline. The small difference in arc length between curve and arc spline has been treated by scaling. Obviously the curvature of each arc segment is constant but the torsion profile of the arc spline needs to be explained. As the arcs are planar curves the torsion is zero at all points except at the junction points where the torsion is not defined. For a sufficiently smooth curve the torsion $\tau(t_0)$ at $\mathbf{g}(t_0)$ can be defined by the limes

$$\tau(t_0) = \lim_{\Delta t \to 0} \frac{\angle \sigma(t_0)\sigma(t_0 + \Delta t)}{\|\dot{\mathbf{g}}(t_0)\|} \tag{4.13}$$

where $\sigma(t)$ denotes the osculating plane at $\mathbf{g}(t)$. At the junction points of the arc spline there is a sudden rotation of the osculating plane around the tangent vector without a change in arc length. We will take over the term *torsion impulse* from Nutbourne [30] for this behavior. We will define such a torsion impulse T at the joining point of two arc segments c_1, c_2 by

$$T = \frac{\angle \sigma_0 \sigma_1}{\frac{1}{2}(l(c_1) + l(c_2))} \tag{4.14}$$

where σ_i are the circles' planes and $l(c_i)$ the arc lengths of the segment c_i.

Example 2 Polynomial curve of degree 4

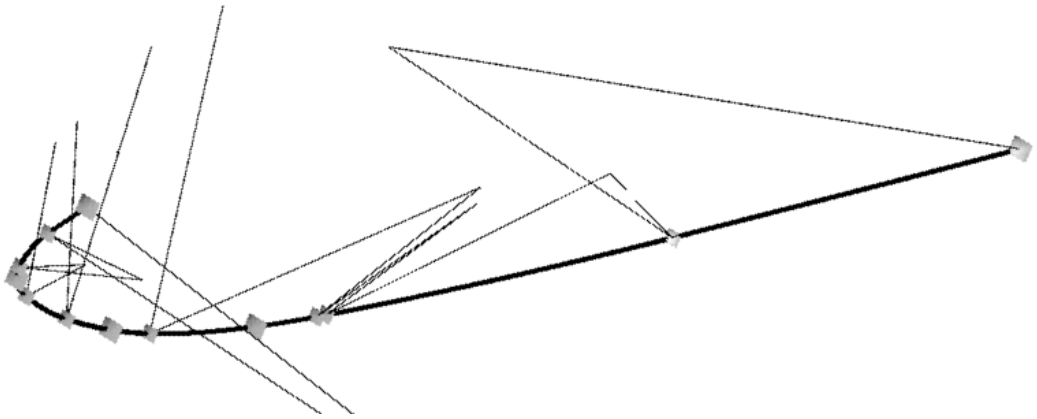

Figure 4.13: Approximation of a polynomial curve of degree 4 with four triarc segments (9 arc segments)

Figure 4.13 shows the arc spline approximation of a polynomial curve of degree 4. The bigger octahedra indicate the position of the segmentation points. These have been chosen at the local minima of the function $F(t)$ (Figure 4.7). After

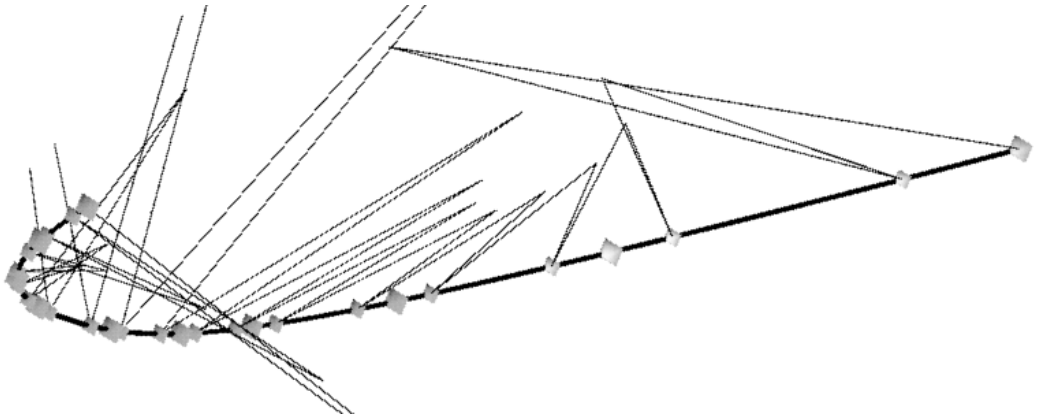

Figure 4.14: Approximation with nine triarc segments (19 arc segments)

further subdivision of the segments as described in section 4.4.2 one obtains an osculating arc spline composed of 19 arc segments. Figure 4.14 gives the final result.

The approximation errors which go with this arc spline are given in Figure 4.15 Note the different scaling of the diagram compared to Fig. 4.8. The maximum absolute error of 0.01 gives a maximum relative error of 0.00025 with respect to the arc length of 40.8 of the whole curve.

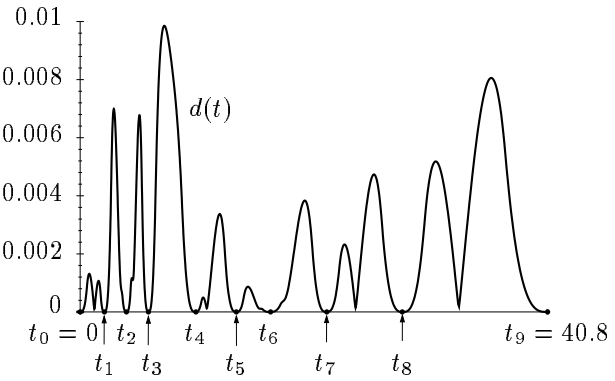

Figure 4.15: Approximation error $d(t)$ for the arc spline approximation of Figure 4.14

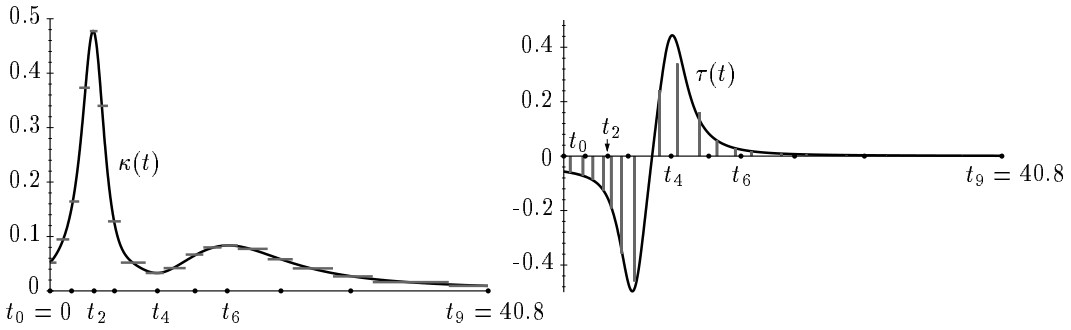

Figure 4.16: (a) Curvature and (b) torsion diagrams of a polynomial curve $\mathbf{g}(t)$ and its arc spline approximation

Figure 4.16(a) gives the curvature diagram of the polynomial curve and the piecewise constant curvature function of the arc spline. Figure 4.16(b) shows the torsion function $\tau(t)$ and the torsion impulses of the approximating arc spline.

Bibliography

[1] Aumann, G., Interpolation with developable Bézier patches, Computer Aided Geometric Design **8** (1991), 409-420.

[2] Aumann, G., A closer look at developable Bézier surfaces, J. of Theoretical Graphics and Computing **7** (1994), 12–26.

[3] Bodduluri, R.M.C. and Ravani, B., Geometric design and fabrication of developable surfaces, ASME Adv. Design Autom. **2** (1992), 243–250.

[4] Bodduluri, R.M.C. and Ravani, B., Design of developable surfaces using duality between plane and point geometries, Computer-Aided Design **25** (1993), 621–632.

[5] Bolton, K.M., Biarc curves, Computer-Aided Design **7** (1975), 89–92.

[6] Cecil, T.E., *Lie Sphere Geometry*, Springer-Verlag, New York 1992.

[7] Chalfant, J.S. and Maekawa, T., Computation of inflection lines and geodesics on developable surfaces, preprint, MIT, 1997.

[8] Chen, H.-Y., Lee, I.-K., Leopoldseder, S., Pottmann, H., Randrup, T. and Wallner, W., On surface approximation using developable surfaces, Technical Report No. 54, Institut für Geometrie, TU Wien, 1998. Accepted for publication in Graphical Models and Image Processing.

[9] Clements, J.C. and Leon, L.J., A fast accurate algorithm for the isometric mapping of a developable surface, SIAM J. Math. Anal. **18** (1987), 966–971.

[10] Farin, G., *Curves and Surfaces for Computer Aided Geometric Design*, Academic Press, Boston, 3rd edn., 1992.

[11] Frey, W.H. and Bindschadler, D., Computer aided design of a class of developable Bézier surfaces, General Motors R&D Publication 8057 (1993).

[12] Fuhs, W. and Stachel, H., Circular pipe connections, Computers & Graphics **12** (1988), 53–57.

[13] Gurunathan, B. and Dhande, S.G., Algorithms for development of certain classes of ruled surfaces, Computers & Graphics **11** (1987), 105–112.

[14] Hoschek, J. and Seemann, G., Spherical splines, Mathematical Modelling and Numerical Analysis **26**, (1992), 1–22.

[15] Hoschek, J., Circular splines, Computer-Aided Design **24** (1992), 611–618.

[16] Hoschek, J., Dual Bézier curves and surfaces, in *Surfaces in Computer Aided Geometric Design*, R.E. Barnhill and W. Boehm, eds., North Holland, 1983, pp. 147–156.

[17] Hoschek, J. and Pottmann, H., Interpolation and approximation with developable B–spline surfaces, in *Mathematical Methods for Curves and Surfaces*, M. Daehlen, T. Lyche and L.L. Schumaker, eds., Vanderbilt University Press, Nashville 1995, pp. 255–264.

[18] Hoschek, J. and Schneider, M., Interpolation and approximation with developable surfaces, in *Curves and Surfaces with Applications in CAGD*, A. Le Méhauté, C. Rabut and L.L. Schumaker, eds., Vanderbilt University Press, Nashville 1997, pp. 185–202.

[19] Kreyszig, E., A new standard isometry of developable surfaces in CAD/CAM, SIAM J. Math. Anal. **25** (1994), 174–178.

[20] Kruppa, E., *Analytische und konstruktive Differentialgeometrie*, Springer-Verlag, Wien 1957.

[21] Lang, J. and Röschel, O., Developable $(1, n)$ Bézier surfaces, Computer Aided Geometric Design **9** (1992), 291–298.

[22] Leopoldseder, S. and Pottmann, H., Approximation of developable surfaces with cone spline surfaces, Computer-Aided Design **30** (1998), 571–582.

[23] Maekawa, T. and Chalfant, J.S., Design and tessellation of B-Spline developable surfaces, preprint, MIT, 1997.

[24] Mancewicz, M.J. and Frey, W.H., Developable surfaces: properties, representations and methods of design, General Motors R&D Publication 7637 (1992).

[25] Meek, D.S. and Walton, D.J., Approximation of discrete data by G^1 arc splines, Computer-Aided Design **24** (1992), 301–306.

[26] Meek, D.S. and Walton, D.J., Approximating quadratic NURBS curves by arc splines, Computer-Aided Design **25** (1993), 371-376.

[27] Meek, D.S. and Walton, D.J., Approximating smooth planar curves by arc splines, J. Computational and Applied Mathematics **59** (1995), 221–231.

[28] Meek, D.S. and Walton, D.J., Planar osculating arc splines, Computer Aided Geometric Design **13** (1996), 653–671.

[29] Müller, E., *Vorlesungen über Darstellende Geometrie, II. Band: Die Zyklographie* (herausgegeben von J.L. Krames), Franz Deuticke, Wien 1929.

[30] Nutbourne, A.W. and Martin, R.R., *Differential Geometry Applied to Curve and Surface Design. Vol. 1: Foundations*, Ellis Horwood, 1988.

[31] Parkinson, D.B. and Moreton, D.N., Optimal biarc-curve fitting, Computer-Aided Design **23** (1991), 411–419.

[32] Parkinson, D.B., Optimized biarc curves with tension, Computer Aided Geometric Design **9** (1992), 207–218.

[33] Piegl, L., Curve fitting algorithm for rough cutting, Computer-Aided Design **18** (1986), 79–82.

[34] Piegl, L. and Tiller, W., *The NURBS Book*, Springer-Verlag, 1995.

[35] Pottmann, H., Studying NURBS curves and surfaces with classical geometry, in *Mathematical Methods for Curves and Surfaces*, M. Daehlen, T. Lyche and L.L. Schumaker, eds., Vanderbilt University Press, Nashville 1995, pp. 413–438.

[36] Pottmann, H., Chen, H.-Y. and Lee, I.-K., Approximation by profile surfaces, in *The Mathematics of Surfaces VIII*, A. Ball et al., eds, Information Geometers Ltd., 1998.

[37] Pottmann, H. and Farin, G., Developable rational Bezier and B–spline surfaces, Computer Aided Geometric Design **12** (1995), 513–531.

[38] Pottmann, H., Lee, I.-K. and Randrup, T., Reconstruction of kinematic surfaces from scattered data, Technical Report No. 48, Institut für Geometrie, TU Wien, 1998.

[39] Pottmann, H. and Randrup, T., Rotational and helical surface approximation for reverse engineering, Computing **60** (1998), 307–322.

[40] Pottmann, H. and Wallner, J., Approximation algorithms for developable surfaces, Technical Report No. 51, Institut für Geometrie, TU Wien, 1998. Accepted for publication in Computer Aided Geometric Design.

[41] Randrup, T., Design and engineering of double-curved ship surfaces, ECMI Newsletter **20** (1996), 18–20.

[42] Redont, P., Representation and deformation of developable surfaces, Computer-Aided Design **21** (1989), 13–20.

[43] Rossignac, J.R. and Requicha, A., Piecewise-circular curves for geometric modeling, IBM J. Res. & Develop. **31** (1987), 296–313.

[44] Sabin, M.A., The use of piecewise forms for the numerical representation of shape, Report 60, Computer and Automation Institute, Hungarian Academy of Sciences, 1977.

[45] Sachs, H., *Isotrope Geometrie des Raumes*, Vieweg, Braunschweig 1990.

[46] Schneider, M., Approximation von Blechhalterflächen mit Torsen in B–Spline Darstellung, Diplomarbeit, TH Darmstadt, 1996.

[47] Schönherr, J., Smooth biarc curves, Computer Aided Design **25** (1993), 365–370.

[48] Seemann, G., Interpolation und Approximation mit sphärischen Kreissplines in Bézier -Darstellung, Diplomarbeit TH Darmstadt.

[49] Seemann, G., Kreissplines und Schraubliniensplines: Interpolation und Approximation durch Raumkurven mit konstanten Invarianten, Dissertation, TH Darmstadt, Shaker, Aachen 1995.

[50] Sharrock, T.J., Biarcs in three dimensions, in *Mathematics of Surfaces II*, R.R. Martin, ed., Oxford University Press, 1986.

[51] Shippey, G.A., Interpolation through a set of data points using circular arc segments, Internal Note Tech/IEG/67/15, Ferranti, Edinburgh 1967.

[52] Su, B-Q. and Liu, D-Y., *Computational Geometry – Curve and Surface Modeling*, Academic Press, Boston 1989.

[53] Sun, M. and Fiume, E., A technique for constructing developable surfaces, Proceedings to Graphics Interface 1996.

[54] Wallner, J., Generalized multiresolution analysis for arc splines, in *Mathematical Methods for Curves and Surfaces II*, M. Daehlen, T. Lyche and L.L. Schumaker, eds., Nashville University Press, 1998, pp. 537–544.

[55] Weiss, G. and Furtner, P., Computer–aided treatment of developable surfaces, Computers & Graphics **12** (1988), 39–51.

[56] Vatter, R., Approximation von Datenpunkten mit Torsen in B–Spline Darstellung, Diplomarbeit, TH Darmstadt, 1996.

Acknowledgements

Here I want to express my sincere thanks to Prof. Helmut Pottmann for supervising this thesis and supporting me with his numerous ideas and comments. I am also grateful to all my colleagues and friends who continuously supported me in my work.

This work has been supported in part by grant No. P12252-MAT of the Austrian Science Foundation.

Vienna, October 1998 Stefan Leopoldseder

Lebenslauf (German)

Am 7. Juli 1971 wurde ich als Sohn des Verschubleiters Johann Leopoldseder und seiner Ehefrau Hermine Leopoldseder, geb. Hackl, in Freistadt/OÖ geboren. Von 1977 bis 1981 besuchte ich die Volksschule in Freistadt, später das Bundesgymnasium in Freistadt, wo ich am 6. Juni 1989 mit Auszeichnung maturierte.

Im Oktober 1989 immatrikulierte ich an der Technischen Universität Wien und inskribierte das Lehramtsstudium für Darstellende Geometrie und Mathematik. Dieses Studium schloß ich am 3. April 1995 mit Auszeichnung ab und am 27. April 1995 wurde mir der akademische Grad eines Magisters der Naturwissenschaften verliehen.

Von April 1993 bis April 1994 war ich am Institut für Mathematik der Universität für Bodenkultur in Wien als Studienassistent tätig. Seit September 1994 bin ich am Institut für Geometrie der TU Wien beschäftigt, zunächst als Studienassistent, seit April 1995 als teilbeschäftigter Vertragsassistent.

Daneben absolvierte ich von September 1995 bis August 1996 das Unterrichtspraktikum am Bundesgymnasium Wien 4, Waltergasse 7. Von September 1996 bis August 1998 unterrichtete ich an der De La Salle Schule Strebersdorf, Wien 21, Anton-Böckgasse 20 und an der HTL Wien 4, Argentinierstraße 11 als teilbeschäftigter Vertragslehrer die Fächer Darstellende Geometrie und Mathematik.

Wien, Oktober 1998 Stefan Leopoldseder